

# NATIONAL ADVISORY COMMITTEE FOR AERONAUTICS

TECHNICAL NOTE 2610

ONE-DIMENSIONAL COMPRESSIBLE FLOW IN VANELESS DIFFUSERS  
OF RADIAL- AND MIXED-FLOW CENTRIFUGAL COMPRESSORS,  
INCLUDING EFFECTS OF FRICTION, HEAT  
TRANSFER AND AREA CHANGE

By John D. Stanitz

Lewis Flight Propulsion Laboratory  
Cleveland, Ohio

PROPERTY FAIRCHILD  
ENGINEERING LIBRARY



Washington  
January 1952

## TECHNICAL NOTE 2610

ONE-DIMENSIONAL COMPRESSIBLE FLOW IN VANELESS DIFFUSERS OF RADIAL-  
AND MIXED-FLOW CENTRIFUGAL COMPRESSORS, INCLUDING EFFECTS  
OF FRICTION, HEAT TRANSFER, AND AREA CHANGE

By John D. Stanitz

## SUMMARY

An analysis method and a design method are developed for one-dimensional, compressible flow with friction, heat transfer, and area change in vaneless diffusers with arbitrary profiles in the axial-radial plane. The effects of mixing losses due to nonuniform flow conditions at the impeller discharge are not considered. In the analysis method the variations in fluid properties, including the velocity and flow direction, are determined as a function of radius for a prescribed variation in diffuser wall spacing with radius. In the design method the variations in effective diffuser wall spacing and in the fluid properties are determined as a function of radius for an arbitrary prescribed variation in one fluid property. For efficient diffuser designs the fluid property selected and the manner in which its variation is prescribed will depend on viscous flow effects that are considered in boundary-layer studies but are not investigated in this report.

As a result of numerical examples it is concluded that: (1) Even with relatively low friction coefficients and neglecting mixing losses near the impeller tip, the friction losses in most vaneless diffuser designs are considerable, as indicated by computed diffuser efficiencies in the low 80's, and these losses result from the usually large ratios of wetted surface to flow area in vaneless diffusers. (2) Vaneless diffuser efficiencies can be improved by increased compressor flow rates for a given impeller tip radius so that the diffuser walls can be spaced farther apart (thus, reducing the ratio of wetted surface to flow area) without increasing the length of the flow path in the diffuser.

## INTRODUCTION

In radial- and mixed-flow centrifugal compressors the vaneless diffuser is an annular duct (fig. 1) immediately following the impeller and of increasing radius in the direction of flow. The high tangential

velocity of the fluid entering the vaneless diffuser from the impeller decreases with increasing radius and, because the tangential velocity is generally the largest velocity component at the impeller discharge, the vaneless diffuser is an effective means of diffusing the fluid, that is, of converting the velocity head to static pressure. The principle by which this conversion is effected is demonstrated by the case for frictionless flow in the absence of heat transfer. For this case, and assuming that flow conditions are uniform in the tangential direction, the moment of momentum of the fluid is constant so that

$$q_{\theta}r = \text{constant}$$

from which as the radius  $r$  increases the tangential velocity  $q_{\theta}$  decreases and therefore the pressure rises (assuming relatively small changes in other components of velocity).

Among the advantages of the vaneless diffuser is the fact that choke flow occurs only if the meridional velocity  $q_m$  (velocity component normal to the annulus area) is sonic. This condition usually corresponds to such high flow rates that choke flow occurs in the impeller, instead of the diffuser as is the usual case for vaned diffusers. The compressor operating range is therefore wider with vaneless diffusers.

Another, and perhaps the most important, advantage of the vaneless diffuser is the fact that if the tangential velocity at the impeller discharge is supersonic the tangential velocity decelerates from supersonic to subsonic velocities without shock losses.

Opposed to these several advantages of the vaneless diffuser is the disadvantage, for aircraft propulsion, of a large frontal area. This disadvantage may be circumvented to some extent by the use of semivaneless diffusers (fig. 2) in which, to diffuse the fluid more rapidly and thus decrease the frontal area of the compressor, vanes are placed in the diffuser following a vaneless section in which the velocity is reduced from supersonic to subsonic magnitudes. Thus, shock losses are avoided by diffusing the flow to subsonic velocities in the vaneless diffuser and the frontal area of the compressor is somewhat reduced by the more rapid diffusion in the vaned section.

In order to analyze the performance of vaneless and semivaneless diffusers and in order to design these diffusers for optimum performance (including the proper setting of the vane angles in semivaneless diffusers), it is necessary to have adequate theoretical methods of predicting the variation in flow characteristics through the diffusers. These methods should include the effects of diffuser geometry, compressibility, heat transfer, friction, and mixing losses caused by the nonuniform flow conditions at the impeller discharge.

Published work on the analysis and design of vaneless and semivaneless diffusers is not extensive (references 1 and 2, for example). In reference 1 a one-dimensional method of analysis is developed for incompressible flow with friction but no mixing losses in vaneless diffusers with constant wall spacing and pure radial flow. In reference 2 a one-dimensional method of design is developed for compressible flow with friction. The method assumes the flow path is a logarithmic spiral and neglects heat transfer and mixing losses.

In the present report methods of analysis and design, carried out at the NACA Lewis laboratory, are developed for one-dimensional, compressible flow with friction, heat transfer, and arbitrary variation in passage height in vaneless diffusers with arbitrary curvature in the meridional (axial-radial) plane. The effect of mixing losses is not considered. In the analysis method and in general for the design method the flow direction, or flow path, is not specified but is a dependent variable determined by the solution. In the design method the variation in diffuser wall spacing with radius is determined for a prescribed variation in one fluid property. For efficient diffuser designs the selection of the one fluid property and its optimum prescribed variation will depend on viscous flow effects that are considered in boundary-layer studies but will not be investigated in this report. The methods are an extension of the work in reference 3 for one-dimensional gas flow in ducts with prescribed flow direction.

#### THEORY OF METHOD

Differential equations are developed that relate the change in dependent variables with radius to the design and operating characteristics of the vaneless diffuser. The application of these differential equations to the analysis of flow in vaneless diffusers and to the design of vaneless diffusers for prescribed distributions of flow conditions with radius is described in a later section.

#### Preliminary Considerations

Coordinate system. - The coordinate system for a point on the mean surface of revolution generated about the axis of the compressor by the center line between the front and rear shroud of the vaneless diffuser is shown in figures 3 and 4. The cylindrical coordinates  $r$ ,  $\theta$ , and  $z$  give the radial, tangential, and axial positions of the point, respectively. The effective diffuser height  $h$  (fig. 3) measured across the passage in the direction normal to the mean surface of revolution is a function of  $r$  only

2391

$$h = h(r) \quad (1)$$

(All symbols are defined in appendix A.) The effective height of the diffuser at each point on the mean surface of revolution is equal to the geometric height of the diffuser minus the assumed displacement thickness of the boundary layer on the diffuser walls. Use of this effective height rather than the geometric height is required by continuity considerations in order to give the proper average value of the velocity component normal to the cross-sectional flow area of the vaneless diffuser. Only the effective height of the diffuser is considered in this report; no investigation is made of the boundary-layer displacement thickness, which can be assumed or estimated from boundary-layer theory.

The slope of the center line between the front and rear shroud of the vaneless diffuser determines the angle  $\alpha$  (fig. 3), which is a function of  $r$  only,

$$\alpha = \tan^{-1} \frac{dr}{dz} = \alpha(r) \quad (2)$$

Assumptions. - The principal assumptions of the analysis and design methods are that flow conditions are uniform across the vaneless diffuser along the height  $h$  and that flow conditions are uniform in the tangential direction  $\theta$ . Thus, the flow becomes one-dimensional, being a function only of the radius along the mean surface of revolution. If the boundary-layer profile is ignored, the accuracy of the assumption that flow conditions may be considered uniform across the vaneless diffuser in the direction of  $h$  depends on: (1) the angle  $\alpha$ , (2) the derivative of  $\alpha$  with respect to  $r$ , (3) the derivative of  $h$  with respect to  $r$ , and (4) the ratio  $h/r$ . For values of  $\alpha$  approximately equal to  $90^\circ$  the assumption is accurate provided  $dh/dr$  and  $d\alpha/dr$  are small. For values of  $\alpha$  less than  $90^\circ$  the inaccuracy of the assumption will depend on the ratio  $h/r$  and the derivative  $d\alpha/dr$ ; for the limiting case in which  $h/r$  and  $d\alpha/dr$  approach zero the assumption is good for all values of  $\alpha$ . In practice the values of  $h/r$  for vaneless diffusers are usually small and the mean shroud curvature  $d\alpha/dr$  should be small to avoid boundary-layer separation. Thus the assumption of uniform flow conditions across the passage along  $h$  should be accurate for all values of  $\alpha$  encountered, except for variations due to the boundary-layer profile.

The motion on the mean surface of revolution is assumed to be steady and, because flow conditions are assumed to be uniform in the tangential direction, mixing losses resulting from nonuniform flow conditions in the tangential direction at the impeller discharge are neglected. These losses are relatively high, but experiments (reference 4,

for example) indicate that they take place in the immediate vicinity of the impeller discharge and may be neglected in the remainder of the vaneless diffuser. The effects of these mixing losses can be accounted for (approximately) by adjustments in the flow conditions (pressure, density, velocity, and flow direction, for example) at the diffuser inlet.

Velocity components. - The velocity  $q$  at a point on the mean surface of revolution is tangent to the surface and has components  $q_r$ ,  $q_\theta$ , and  $q_z$  in the  $r$ -,  $\theta$ -, and  $z$ -directions, respectively. In this analysis it is convenient to consider the meridional velocity  $q_m$  (instead of  $q_r$  and  $q_z$ ), which is tangent to the center line between the front and rear shroud of the diffuser in the meridional plane (fig. 3) and is related to  $q_r$  and  $q_z$  by

$$q_m = \sqrt{q_r^2 + q_z^2} \quad (3)$$

The flow direction  $\beta$  on the mean surface of revolution is related to  $q_m$  and  $q_\theta$  by (fig. 5)

$$\tan \beta = \frac{q_\theta}{q_m} \quad (4a)$$

from which

$$q_\theta = q \sin \beta \quad (4b)$$

$$q_m = q \cos \beta \quad (4c)$$

Fluid particle. - A fluid particle on the mean surface of revolution is shown in figure 4. This particle has the dimensions  $r d\theta$  and  $dr/\sin \alpha$  on the surface of revolution and the height  $h$  normal to the surface.

Outline of method. - The state of the fluid at any point ( $r$ ) on the mean surface of revolution is described by three thermodynamic properties, by the fluid velocity, and by the flow direction. These five properties can be determined from five fundamental relations: (1) continuity, (2) equilibrium in the direction of  $q_m$  (meridional equilibrium), (3) equilibrium in the direction of  $q_\theta$  (tangential equilibrium), (4) equation of state, and (5) the heat-transfer equation. In

addition to these five fundamental relations certain definitions are required to express the resulting equations in terms of the desired properties. The properties that will be used in this analysis to describe the state of the fluid will be the static pressure  $p$ , the static density  $\rho$ , the total temperature  $T_t$ , the local Mach number  $M$ , and the flow direction  $\beta$ .

Mach number. - The local Mach number  $M$  is defined by

$$M^2 = \frac{q^2}{\gamma g R^* T} \quad (5)$$

where  $\gamma$  is the ratio of specific heats,  $g$  is the gravitational acceleration,  $R^*$  is the gas constant, and  $T$  is the local, static temperature. From equation (5)

$$\frac{1}{M^2} \frac{dM^2}{dr} = \frac{1}{q^2} \frac{dq^2}{dr} - \frac{1}{T} \frac{dT}{dr} \quad (5a)$$

Total temperature. - The total temperature  $T_t$  is defined by

$$T_t = T + \frac{q^2}{2Jgc_p}$$

or

$$T_t = T \left( 1 + \frac{\gamma-1}{2} M^2 \right) \quad (6)$$

where  $J$  is the mechanical equivalent of heat and  $c_p$  is the specific heat at constant pressure. From equation (6)

$$\frac{1}{T_t} \frac{dT_t}{dr} = \frac{1}{T} \frac{dT}{dr} + \left( \frac{\frac{\gamma-1}{2} M^2}{1 + \frac{\gamma-1}{2} M^2} \right) \frac{1}{M^2} \frac{dM^2}{dr} \quad (6a)$$

From equations (5a) and (6a)

$$\frac{1}{q^2} \frac{dq^2}{dr} = \left( \frac{1}{1 + \frac{\gamma-1}{2} M^2} \right) \frac{1}{M^2} \frac{dM^2}{dr} + \frac{1}{T_t} \frac{dT_t}{dr} \quad (6b)$$

Fundamental Relations

Continuity. - The continuity equation for one-dimensional compressible flow in vaneless diffusers is

$$\rho q_m r h = \text{constant}$$

from which

$$\frac{1}{\rho} \frac{d\rho}{dr} + \frac{1}{q_m} \frac{dq_m}{dr} + \frac{1}{h} \frac{dh}{dr} + \frac{1}{r} = 0 \quad (7)$$

where changes in  $r$  are understood to occur along the mean surface of revolution.

Meridional equilibrium. - The equation for meridional equilibrium of a fluid particle (fig. 6) in the direction of  $q_m$  on the mean surface of revolution is obtained from a balance of the pressure forces, shear forces, and inertia forces (appendix B)

$$\frac{g}{\rho} \frac{d\rho}{dr} + \frac{c_f q^2 \cos \beta}{h \sin \alpha} = \frac{q_\theta^2}{r} - q_m \frac{dq_m}{dr} \quad (8)$$

where  $c_f$  is the skin-friction coefficient.

Tangential equilibrium. - The equation for tangential equilibrium of the fluid particle in figure 6 is obtained from a balance of the shear forces and the inertia forces (appendix B)

$$-\frac{c_f q^2 \sin \beta}{h \sin \alpha} = q_m \frac{dq_\theta}{dr} + \frac{q_m q_\theta}{r} \quad (9)$$

Equation of state. - By definition a perfect gas satisfies the equation of state

2391

$$p = \rho R^* T \quad (10a)$$

from which

$$\frac{1}{p} \frac{dp}{dr} = \frac{1}{\rho} \frac{d\rho}{dr} + \frac{1}{T} \frac{dT}{dr} \quad (10b)$$

Heat-transfer equation. - The heat-transfer rate to the diffuser casing must equal the heat-transfer rate from the fluid. The heat-transfer rate to the diffuser casing is given approximately by

$$dQ = 2h' (T_w - T_t) 2\pi r \frac{dr}{\sin \alpha} \quad (11a)$$

where  $h'$  is the coefficient of heat transfer,  $T_w$  is the wall, or diffuser casing, temperature, and  $dQ$  is the heat-transfer rate. Equation (11a) assumes that the recovery factor at the wall is 1.0 (reference 3, p. A-328).

The heat-transfer rate from the fluid is given approximately by

$$dQ = \rho q_m 2\pi r h c_p \frac{dT_t}{dr} dr \quad (11b)$$

Finally, from equations (11a) and (11b)

$$\frac{1}{T_t} \frac{dT_t}{dr} = \frac{2h'}{\rho q_m h c_p \sin \alpha} \left( \frac{T_w}{T_t} - 1 \right) \quad (11c)$$

Equation (11c) gives the change in total temperature with radius as a function of the heat-transfer coefficient  $h'$ .

Reynolds' analogy. - An approximate value for  $h'$  in equation (11c) can be obtained from the Reynolds' analogy between friction and heat transfer (reference 3)

$$\frac{h'}{c_p \rho q} = \frac{c_f}{2}$$

From which equation (11c) becomes

$$\frac{1}{T_t} \frac{dT_t}{dr} = \frac{c_f \sec \beta}{h \sin \alpha} \left( \frac{T_w}{T_t} - 1 \right) \quad (12)$$

Equation (12) gives the change in total temperature with radius as a function of the skin-friction coefficient and the ratio of wall temperature to total temperature of the fluid.

Review. - A review of the theory up to this point indicates nine unknowns and nine equations for the analysis method. The unknowns are:  $p$ ,  $\rho$ ,  $T$ ,  $T_t$ ,  $M$ ,  $q$ ,  $q_m$ ,  $q_\theta$ , and  $\beta$ . (For the design method  $h$  is unknown and replaces one of these nine quantities, which is then specified as a function of  $r$ . The angle  $\alpha$  is a known function of  $r$  for both analysis and design methods.) The nine equations are:

	Equation
Tangential velocity	(4b)
Meridional velocity	(4c)
Mach number (definition)	(5a)
Total temperature (definition)	(6a)
Continuity	(7)
Meridional equilibrium	(8)
Tangential equilibrium	(9)
Equation of state	(10b)
Heat-transfer equation	(11c) or (12)

The solution for the analysis method consists in combining the nine equations to obtain three differential equations involving three unknowns:  $T_t$ ,  $M$ , and  $\beta$ . These three differential equations, in turn, can be combined to solve, by numerical methods, for  $T_t$ ,  $M$ , and  $\beta$  successively. (For the design method an auxiliary equation is developed for  $\frac{1}{h} \frac{dh}{dr}$  in terms of the prescribed fluid property as a function of  $r$ . The three unknowns  $T_t$ ,  $M$ , and  $\beta$  are then obtained in the same manner outlined for the analysis method.)

#### Final Equations

Auxiliary differential equation. - An auxiliary differential equation for the pressure  $p$  in terms of  $T_t$ ,  $M$ , and  $\beta$  is obtained from the equilibrium equations, which, after expressing  $q_\theta$  and  $q_m$  in terms of  $q$  and  $\beta$ , combine to give

$$\frac{g}{\rho q^2} \frac{dp}{dr} = - \frac{1}{2q^2} \frac{dq^2}{dr} - \frac{c_f \sec \beta}{h \sin \alpha} \quad (13a)$$

But,

$$\frac{\rho q^2}{g} = \frac{\gamma p q^2}{\gamma g R^* T} = \gamma p M^2 \quad (13b)$$

so that, from equations (6b), (13a), and (13b)

$$\frac{1}{P} \frac{dP}{dR} = - \frac{\gamma M^2}{2} \left[ \left( \frac{1}{1 + \frac{\gamma-1}{2} M^2} \right) \frac{1}{M^2} \frac{dM^2}{dR} + \frac{1}{T_t} \frac{dT_t}{dR} + \frac{2\zeta}{H \cos \beta} \right] \quad (13c)$$

where

$$\zeta = \frac{c_f}{\sin \alpha} \left( \frac{r_T}{h_T} \right) \quad (13d)$$

and where

$$\left. \begin{aligned} P &= \frac{p}{p_0} \\ R &= \frac{r}{r_T} \\ H &= \frac{h}{h_T} = H(R) \end{aligned} \right\} \quad (13e)$$

where  $p_0$  is the compressor-inlet stagnation pressure,  $r_T$  is the impeller tip radius, and  $h_T$  is the effective diffuser height at the impeller tip. Equation (13c) is an auxiliary differential equation that relates the change in  $P$  to the change in  $T_t$  and  $M^2$  with radius  $R$ .

Total temperature. - The change in  $T_t$  is given by equation (11c) or (12), which from equations (13d) and (13e) become

$$\frac{1}{T_t} \frac{dT_t}{dR} = \frac{2h'}{\rho q_m H c_p \sin \alpha} \left( \frac{T_w}{T_t} - 1 \right) \frac{r_T}{h_T} \quad (14a)$$

and, for the case of Reynolds' analogy,

$$\frac{1}{T_t} \frac{dT_t}{dR} = \frac{\zeta}{H \cos \beta} \left( \frac{T_w}{T_t} - 1 \right) \quad (14b)$$

Mach number. - In order to determine the differential equation for the Mach number squared it is first necessary to express the second term of the continuity equation (7) in terms of known variables. From the meridional equilibrium equation (8) together with equations (4) and (13b)

$$\frac{1}{q_m} \frac{dq_m}{dr} = \frac{\tan^2 \beta}{r} - \frac{\sec^2 \beta}{\gamma M^2} \frac{1}{p} \frac{dp}{dr} - \frac{c_f \sec \beta}{h \sin \alpha} \quad (15a)$$

The first term of the continuity equation (7) is expressed in terms of known variables by the equation of state (10b) together with equation (6a)

$$\frac{1}{\rho} \frac{d\rho}{dr} = \frac{1}{p} \frac{dp}{dr} - \frac{1}{T_t} \frac{dT_t}{dr} + \left( \frac{\frac{\gamma-1}{2} M^2}{1 + \frac{\gamma-1}{2} M^2} \right) \frac{1}{M^2} \frac{dM^2}{dr} \quad (15b)$$

Substituting equations (15a) and (15b) into the continuity equation (7) and combining it with equations (13d) and (13e) result in

$$\frac{1}{P} \frac{dP}{dR} = \frac{-\gamma M^2}{\gamma M^2 - \sec^2 \beta} \left[ \left( \frac{\frac{\gamma-1}{2} M^2}{1 + \frac{\gamma-1}{2} M^2} \right) \frac{1}{M^2} \frac{dM^2}{dR} - \frac{1}{T_t} \frac{dT_t}{dR} - \frac{\zeta}{H \cos \beta} + \frac{1}{H} \frac{dH}{dR} + \frac{\sec^2 \beta}{R} \right]$$

which, combined with equation (13c) to eliminate  $\frac{1}{P} \frac{dP}{dR}$ , finally gives

$$\frac{1}{M^2} \frac{dM^2}{dR} = \frac{-2 \left( 1 + \frac{\gamma-1}{2} M^2 \right)}{M^2 - \sec^2 \beta} \left[ (1 + \gamma M^2 - \tan^2 \beta) \frac{1}{2T_t} \frac{dT_t}{dr} + \right. \\ \left. (\gamma M^2 - \tan^2 \beta) \frac{\xi}{H \cos \beta} - \frac{1}{H} \frac{dH}{dR} - \frac{\sec^2 \beta}{R} \right] \quad (15c)$$

Equation (15c) determines the change in  $M^2$  with radius  $R$  along the mean surface of revolution in terms of  $\frac{1}{T_t} \frac{dT_t}{dR}$ , which is known from equations (14a) or (14b).

Flow direction. - The differential of the flow direction  $\beta$  is obtained from equation (4a)

$$\frac{1}{\tan \beta} \frac{d \tan \beta}{dr} = \frac{1}{q_\theta} \frac{dq_\theta}{dr} - \frac{1}{q_m} \frac{dq_m}{dr}$$

which from the tangential equilibrium equation (9) and equation (15a) becomes

$$\frac{1}{\tan \beta} \frac{d \tan \beta}{dR} = \frac{\sec^2 \beta}{\gamma M^2} \frac{1}{P} \frac{dP}{dR} - \frac{\sec^2 \beta}{R}$$

and from equations (13c) and (15c)

$$\frac{1}{\tan \beta} \frac{d \tan \beta}{dR} = \frac{\sec^2 \beta}{M^2 - \sec^2 \beta} \left\{ \left( 1 + \frac{\gamma-1}{2} M^2 \right) \frac{1}{T_t} \frac{dT_t}{dR} + \right. \\ \left. \left[ 1 + (\gamma-1) M^2 \right] \frac{\xi}{H \cos \beta} - \frac{1}{H} \frac{dH}{dR} - \frac{M^2}{R} \right\} \quad (16)$$

Equations (14a) or (14b), (15c), and (16) are three differential equations that can be solved simultaneously for  $T_t$ ,  $M^2$ , and  $\beta$ .

Pressure. - After the variations in  $T_t$ ,  $M^2$ , and  $\beta$  with radius  $R$  are known the pressure  $P$  can be obtained from the continuity equation as follows:

$$\rho_1 q_1 \cos \beta_1 r_{T^h_T} = \rho q \cos \beta rh \quad (17a)$$

where the subscript 1 refers to known conditions (appendix C) at the diffuser inlet (where  $R$  is equal to 1.0). From the equation of state (10a) and from the definition of Mach number (equation (5)), equation (17a) becomes

$$\frac{P_1}{T_1} M_1 \sqrt{T_1} \cos \beta_1 r_{T^h_T} = \frac{P}{T} M \sqrt{T} \cos \beta rh$$

Finally, from equations (6) and (13e)

$$\frac{P}{P_1} = \frac{1 \cos \beta_1 M_1}{RH \cos \beta M} \sqrt{\frac{T_t \left(1 + \frac{\gamma-1}{2} M_1^2\right)}{(T_t)_1 \left(1 + \frac{\gamma-1}{2} M^2\right)}} \quad (17b)$$

Equation (17b) determines  $P$  from the known conditions at the diffuser inlet and from the known values of  $T_t$ ,  $M^2$ , and  $\beta$  determined by the simultaneous solution of equations (14a) or (14b), (15c), and (16).

After the quantities  $P$ ,  $M^2$ ,  $T_t$ , and  $\beta$  are known, all other quantities ( $\rho$ ,  $T$ ,  $q$ ,  $q_m$ , and  $q_\theta$ ) can be determined directly from equations (4), (5), (6), and the equation of state (10a).

Flow path. - The flow path on the mean surface of revolution in the vaneless diffuser can be obtained from the known variation in  $\tan \beta$  with  $R$  given by the solution of equation (16). From figure 7, which shows the flow path on a developed view of the mean surface in the vicinity of  $R$ ,

$$\tan \beta = \frac{R d\theta}{dR/\sin \alpha}$$

or

$$\frac{d\theta}{dR} = \frac{\tan \beta}{R \sin \alpha} \quad (18)$$

Because  $\beta$  and  $\alpha$  are known functions of  $R$ , equation (18) determines the flow path on the mean surface of revolution.

Influence coefficients. - In some analysis problems it may be convenient or desirable to solve directly for one or more of the other dependent quantities rather than  $T_t$ ,  $M^2$ , and  $\beta$ . Also, in the design problem it may be desired to specify one of these quantities as a function of  $R$  and to solve for the required value of  $\frac{1}{H} \frac{dH}{dR}$ . For these cases the change in the dependent variables  $P$ ,  $\rho$ ,  $T$ ,  $q$ ,  $q_m$ , and  $q_\theta$  with radius  $R$  along the mean surface of revolution, as well as the change in  $T_t$ ,  $M^2$ , and  $\beta$ , must be expressed in terms of the known quantities  $\frac{1}{T_t} \frac{dT_t}{dR}$  (given by equations (14a) or (14b)),  $\frac{\xi}{H \cos \beta}$ ,  $\frac{1}{R}$ , and  $\frac{1}{H} \frac{dH}{dR}$  (not known in the design problem), which quantities are multiplied by influence coefficients. Thus, if  $X$  is any one of the dependent variables,

$$(M^2 - \sec^2 \beta) \frac{1}{X} \frac{dX}{dR} = I_1 \left( 1 + \frac{\gamma-1}{2} M^2 \right) \frac{1}{T_t} \frac{dT_t}{dR} + I_2 \frac{\xi}{H \cos \beta} + I_3 \frac{1}{H} \frac{dH}{dR} + I_4 \frac{1}{R} \quad (19)$$

where  $I_1$  through  $I_4$  are influence coefficients that are determined in the same way that equations (15c) and (16) were developed. The influence coefficients for various dependent variables  $X$  are given in the following table:

X	Influence Coefficients			
	$I_1$	$I_2$	$I_3$	$I_4$
P	$\gamma M^2$	$\gamma M^2 [1 + (\gamma-1)M^2]$	$-\gamma M^2$	$-\gamma M^2 \sec^2 \beta$
$\rho$	$\sec^2 \beta$	$M^2 (\gamma \sec^2 \beta - \tan^2 \beta)$	$-M^2$	$-M^2 \sec^2 \beta$
T	$\gamma M^2 - \sec^2 \beta$	$(\gamma-1)M^2 (\gamma M^2 - \tan^2 \beta)$	$-(\gamma-1)M^2$	$-(\gamma-1)M^2 \sec^2 \beta$
$M^2$	$\tan^2 \beta - 1 - \gamma M^2$	$2 \left( 1 + \frac{\gamma-1}{2} M^2 \right) (\tan^2 \beta - \gamma M^2)$	$2 \left( 1 + \frac{\gamma-1}{2} M^2 \right)$	$2 \left( 1 + \frac{\gamma-1}{2} M^2 \right) \sec^2 \beta$
$q^2$	-2	$2 (\tan^2 \beta - \gamma M^2)$	2	$2 \sec^2 \beta$
$q_m$	$-\sec^2 \beta$	$M^2 (\tan^2 \beta - \gamma \sec^2 \beta)$	$\sec^2 \beta$	$\sec^2 \beta + M^2 \tan^2 \beta$
$q_\theta$	0	$\sec^2 \beta - M^2$	0	$\sec^2 \beta - M^2$
$\tan \beta$	$\sec^2 \beta$	$\sec^2 \beta [1 + (\gamma-1)M^2]$	$-\sec^2 \beta$	$-M^2 \sec^2 \beta$

If  $M^2$  is equal to  $\sec^2\beta$ , the left side of equation (19) is equal to zero because  $\frac{1}{X} \frac{dX}{dR}$  cannot be infinite. For this condition ( $M^2 = \sec^2\beta$ ), which occurs when  $q_m$  is equal to the local speed of sound, that is when choke flow occurs (appendix D), equation (19) becomes

$$\left(1 + \frac{\gamma-1}{2} \sec^2\beta\right) \frac{1}{T_t} \frac{dT_t}{dR} + \left[1 + (\gamma-1) \sec^2\beta\right] \frac{\xi}{H \cos \beta} - \frac{1}{H} \frac{dH}{dR} - \frac{\sec^2\beta}{R} = 0 \quad (19a)$$

where the influence coefficients given in the table have been substituted in equation (19) with  $M^2$  equal to  $\sec^2\beta$ . (All sets of influence coefficients result in the same equation (19a).) Equation (19a) is a condition that must be satisfied at the location of choke flow in a vaneless diffuser. In particular, if heat transfer and friction are absent, equation (19a) becomes

$$\frac{1}{HR} \frac{d(HR)}{dR} = \frac{-\tan^2\beta}{R}$$

Because  $HR$  is directly proportional to the flow area, it is seen that choke flow does not occur at the throat, or position of minimum flow area ( $\frac{d(HR)}{dR} = 0$ ), but at a point where the flow area is decreasing in the direction of increasing  $R$ .

Small-stage efficiency. - The small-stage, or polytropic, efficiency at a given radius  $R$  on the mean surface of revolution in a vaneless diffuser is defined as the ratio of the ideal (ignoring friction and heat transfer) to the actual differential change in static enthalpy with radius required to accomplish the actual differential change in static pressure with radius. This definition leads to the following expression for the small-stage efficiency  $\eta$  (appendix E)

$$\eta = \frac{\frac{1}{P} \frac{dP}{dR}}{\frac{1}{P} \frac{dP}{dR} + \frac{\gamma}{\gamma-1} \left(1 + \frac{\gamma-1}{2} M^2\right) \frac{1}{T_t} \frac{dT_t}{dR} + \frac{\gamma M^2 \xi}{H \cos \beta}} \quad (20a)$$

Equation (20a) indicates that in the absence of heat transfer ( $\frac{dT_t}{dR} = 0$ ) and friction ( $\xi = 0$ ) the small-stage efficiency is 100 percent. Also, for heat transfer from the fluid to the diffuser walls,

$\frac{1}{T_t} \frac{dT_t}{dR}$  is negative and therefore results in an apparent increase in the small-stage efficiency. Thus, in the presence of heat transfer, the small-stage efficiency, as just defined, is not a good measure of the performance of vaneless diffusers in that it is not a measure of the magnitude of the losses involved. In the absence of heat transfer  $\frac{dT_t}{dR}$  is zero and equation (20a) can be rearranged to give (appendix E)

$$\eta = 1 - \frac{\xi (M^2 - \sec^2 \beta)}{\xi (\gamma M^2 - \tan^2 \beta) - \cos \beta \left( \frac{dH}{dR} + \frac{H \sec^2 \beta}{R} \right)} \quad (20b)$$

If  $M^2$  is equal to  $\sec^2 \beta$  (choke flow condition, appendix D), the efficiency given by equation (20b) becomes indeterminate, because the numerator of the fraction is zero and, from equation (19a), so is the denominator.

#### NUMERICAL PROCEDURE

A specific numerical procedure is outlined for both the analysis and design problems, however, any other standard numerical procedure can be used. In the analysis problem the variation in fluid properties with  $R$  are determined for a specified geometry of the vaneless diffuser. In the design problem the variation with  $R$  in one of the fluid properties is prescribed and the remaining fluid properties together with the variation in diffuser height  $H$  with radius  $R$  are determined. The numerical procedures for both the analysis and design problems are essentially the same but differ in detail and are therefore discussed separately in this section.

#### Analysis Problem

Primary quantities. - In the analysis problem the variation with  $R$  in three primary quantities ( $T_t$ ,  $M^2$ , and  $\beta$ ) are obtained from three differential equations: (14a) or (14b), (15c), and (16). These equations are nonlinear and it is necessary to solve them by numerical methods. The suggested stepwise procedure is as follows:

- (1) The values of  $T_t$ ,  $M^2$ , and  $\beta$  at the diffuser inlet are estimated from the impeller design and operating characteristics (appendix C).

(2) At any radius  $R$ , if  $T_t$ ,  $M^2$ , and  $\tan \beta$  are known, the change in  $T_t$  (that is,  $\Delta T_t$ ) for a small increase in  $R$  (that is,  $\Delta R$ ) is computed directly from equation (14a) or (14b).

(3) The change in  $M^2$  (that is,  $\Delta M^2$ ) for the same small change in  $R$  (that is,  $\Delta R$ ) is computed directly from equation (15c) in which  $\frac{1}{T_t} \frac{dT_t}{dR}$  is obtained from step (2).

(4) Finally  $\Delta \tan \beta$  is computed from equation (16).

(5) Thus, at  $(R + \Delta R)$  the approximate values of  $T_t$ ,  $M^2$ , and  $\tan \beta$  are known from the values of  $T_t$ ,  $M^2$ , and  $\tan \beta$  at  $R$  and the approximate values of  $\Delta T_t$ ,  $\Delta M^2$ , and  $\Delta \tan \beta$  given by steps (2) through (4).

(6) At  $(R + \Delta R)$  approximate values of  $\frac{1}{T_t} \frac{dT_t}{dR}$ ,  $\frac{1}{M^2} \frac{dM^2}{dR}$ , and  $\frac{1}{\tan \beta} \frac{d \tan \beta}{dR}$  can then be determined by equations (14a) or (14b), (15c), and (16) from the approximate values of  $T_t$ ,  $M^2$ , and  $\tan \beta$  obtained in step (5).

(7) The final values of  $\Delta T_t$ ,  $\Delta M^2$ , and  $\Delta \tan \beta$  between  $R$  and  $(R + \Delta R)$  are obtained directly from the arithmetic average of  $\frac{1}{T_t} \frac{dT_t}{dR}$ , and so forth, at  $R$  and  $(R + \Delta R)$  as given in steps (2), (3), (4), and (6).

(8) The values of  $T_t$ ,  $M^2$ , and  $\tan \beta$  at  $(R + \Delta R)$  are determined from the known values of  $T_t$ ,  $M^2$ , and  $\tan \beta$  at  $R$  and from the values of  $\Delta T_t$ ,  $\Delta M^2$ , and  $\Delta \tan \beta$  obtained in step (7).

(9) The stepwise procedure outlined in steps (2) through (8) is repeated for small values of  $\Delta R$  starting at  $R$  equal to 1.0 (where  $T_t$ ,  $M^2$ , and  $\tan \beta$  are obtained by step (1)) and continuing to the diffuser exit. For the numerical examples of this report  $\Delta R$  was 0.02, 0.03, and 0.05 for the first three increments and 0.10 for the remaining.

Secondary quantities. - After the distribution of  $T_t$ ,  $M^2$ , and  $\tan \beta$  with  $R$  are known, the distribution of  $P$ ,  $\rho$ ,  $T$ ,  $q$ ,  $q_m$ , and  $q_\theta$  can be determined directly from equation (17b) and from equation (4), (5), (6), and the equation of state (10a).

Flow path. - The flow path on the mean surface of revolution in the vaneless diffuser is given by  $\theta$  as a function of  $R$  along the surface. Because  $\tan \beta$  and  $\sin \alpha$  are known functions of  $R$ , the flow path ( $\theta = \theta(R)$ ) can be determined by the numerical integration of equation (18) assuming  $\theta$  equals zero at  $R$  equals 1.0.

Efficiency. - The small-stage, or polytropic, efficiency  $\eta$  at each radius  $R$  is given by equation (20a). The diffuser efficiency  $(\eta_D)_R$  between radius  $R$  equals 1.0 and  $R$  is given by equation (E6) in appendix E.

### Design Problem

In the design method the variation in effective diffuser wall spacing with radius is determined for a prescribed variation in one fluid property. For efficient diffuser designs the selection of the one fluid property and its optimum prescribed variation will depend on viscous flow effects that are considered in boundary-layer studies but will not be investigated in this report. (Nor is the magnitude of the boundary-layer displacement, required to obtain the geometric wall spacing from the effective spacing, considered in this report.)

Auxiliary equation. - In the design problem the variation in  $H$  with  $R$  is unknown and must be determined to satisfy a specified variation in one characteristic of the flow ( $q_m$ , for example) with  $R$ . From this specified variation in one characteristic of the flow  $\frac{1}{H} \frac{dH}{dR}$  can be determined from equation (19). The quantity  $\Delta H$  between  $R$  and  $(R + \Delta R)$  is obtained from the average value of  $\frac{1}{H} \frac{dH}{dR}$  at  $R$  and  $(R + \Delta R)$ . After  $H$  has been determined at  $(R + \Delta R)$  the final values of  $\Delta T_t$ ,  $\Delta M^2$ ,  $\Delta P$ , and  $\Delta \tan \beta$  between  $R$  and  $(R + \Delta R)$  are obtained by the same procedure previously outlined for the analysis problem. The process starts at  $R$  equals 1.0 (where  $H$  equals 1.0) and is repeated for specified increments of  $R$  up to the diffuser exit.

Complete solution. - After the variation in  $H$ ,  $T_t$ ,  $M^2$ , and  $\tan \beta$  with  $R$  are known, the variation in  $P$ ,  $\rho$ ,  $T$ ,  $q$ ,  $q_m$ , and  $q_\theta$  can be determined directly from equation (17b) and from equations (4), (5), (6), and the equation of state (10a). The flow path is determined by equation (18) as outlined previously, and the small-stage, or polytropic, efficiency is determined by equation (20a).

### NUMERICAL EXAMPLES

The numerical examples of this report are divided into three groups: (1) effects of some operating conditions, (2) effects of diffuser wall spacing, and (3) a vaneless diffuser design problem.

Effects of Some Operating Conditions

The first group of numerical examples shows the effects of heat transfer and friction on the flow in vaneless diffusers. Three numerical examples are given: (1) isentropic compressible flow, (2) compressible flow with friction, and (3) compressible flow with friction and heat transfer.

Inlet conditions. - For the first group of numerical examples the flow conditions at the diffuser inlet ( $R = 1.0$ ) are:

$$P_1 = 3.022$$

$$M_1^2 = 1.370$$

$$(T_t)_1 = 941^\circ R$$

$$(\tan \beta)_1 = 3.829$$

These conditions were estimated (by methods given in appendix C) for the following design and operating conditions of the impeller:

Compressor flow coefficient, $\phi$ . . . . .	0.75
Impeller tip Mach number, $M_T$ . . . . .	1.5
Impeller slip factor, $\mu$ . . . . .	0.9
Impeller polytropic efficiency, $\eta$ . . . . .	0.9
Compressor stagnation inlet temperature, $T_o$ , $^\circ R$ . . . . .	520

Diffuser design. - The design characteristics of the diffuser are:

Passage height, $H$ . . . . .	$R^{-1}$
(constant flow area normal to $q_m$ )	
Wall temperature, $T_w$ , $^\circ R$ . . . . .	750
Friction parameter, $\xi$ . . . . .	0.030

$$\left[ \begin{array}{l} c_f = 0.003 \text{ (a relatively low value, see reference 4)} \\ \frac{1}{\sin \alpha} \left( \frac{r_T}{h_T} \right) = 10 \text{ (so that } \sin \alpha \text{ is constant)} \end{array} \right]$$

The Reynolds' analogy was used to determine the heat-transfer coefficient so that equation (12) was used to determine the change in total temperature with radius.

Results. - The results of the first group of three numerical examples are given in figure 8. In figure 8(a) is shown the change in  $M^2$  with  $R$  for the three numerical examples. The effect of friction is to reduce  $M^2$  at each radius  $R$  (because, although the smaller meridional velocity component  $q_m$  is increased as usual, the larger

2391

tangential component  $q_\theta$  is decreased) and the effect of heat transfer from the fluid is to increase  $M^2$  slightly (primarily because of the reduced speed of sound at the lower temperature) for the magnitudes of  $T_t$  and  $T_w$  involved in these examples.

In figure 8(b) is shown the change in  $P$  with  $R$ . As expected, the effect of friction is to reduce  $P$  at each radius (primarily because of the decreased values of  $q_\theta$ , which require a smaller pressure gradient for equilibrium). The effect of heat transfer from the fluid is to raise  $P$  slightly for the magnitudes of  $T_t$  and  $T_w$  involved in these examples.

In figure 8(c) is shown the change in flow direction  $\beta$  with  $R$ . The effect of friction is to reduce  $\beta$  because  $q_\theta$  is reduced and  $q_m$  is increased to satisfy continuity with lower density due to lower  $P$ . The effect of heat transfer from the fluid is to increase  $\beta$  slightly because of the reduced value of  $q_m$  resulting from the increased value of  $\rho$ .

In figure 8(d) is shown the flow path in the vaneless diffuser. The effect of friction is to shorten the flow path because  $\beta$  is decreased (fig. 8(c)). The effect of heat transfer is to lengthen the path slightly.

In figure 8(e) is shown the change in polytropic, or small-stage, efficiency  $\eta$  with radius  $R$ . The effect of friction is to reduce the efficiency at each radius. The effect of heat transfer from the fluid is to increase  $\eta$  greatly. In fact for the larger values of  $R$  where  $M^2$  is relatively small the term involving  $\frac{1}{T_t} \frac{dT_t}{dR}$  becomes greater than the term involving the friction parameter  $\zeta$  (see equation (20a)) and, because for heat transfer from the fluid  $\frac{1}{T_t} \frac{dT_t}{dR}$  is negative,  $\eta$  becomes greater than 100 percent.

For the example with friction but no heat transfer it is interesting to note that, although the friction losses must be greater at the lower values of  $R$  because of the larger velocities, the polytropic efficiency is higher. From equation (20a) the higher efficiency must result from a higher rate of pressure rise  $\frac{1}{P} \frac{dP}{dR}$  compared with  $\frac{\gamma M^2 \zeta}{H \cos \beta}$  at the lower values of  $R$ . In current compressor designs the local polytropic efficiency at the lower values of  $R$  will be considerably reduced (reference 4, for example) because of mixing losses resulting from the nonuniform flow conditions at the impeller discharge.

The diffuser efficiency  $(\eta_D)_2$  at  $R$  equal to 2.0 is determined by equation (E6) of appendix E and is indicated for each of the three numerical examples in figure 8(e). The value of  $(\eta_D)_2$ , for the example with heat transfer, is considerably less than the values of the polytropic efficiency  $\eta$  at the larger values of  $R$  for this example, because for these larger values of  $R$  the rate of pressure rise is smaller and therefore  $\eta$  has less effect upon the value of  $(\eta_D)_2$ . Even so, the value of  $(\eta_D)_2$  for the example with friction and heat transfer is almost 100 percent. But from figure 8(b) the pressure  $P$  at  $R$  equal to 2.0 is not much different for the two examples with and without heat transfer (but with friction) so that the losses are about equal for these examples and  $(\eta_D)_2$ , which is considerably different, is therefore not a reliable measure of the losses when heat transfer effects are present.

For the example with friction and no heat transfer the value of  $(\eta_D)_2$  is as low as 0.824 in spite of the relatively low friction coefficient ( $c_f = 0.003$ ) and in spite of neglecting the mixing losses due to nonuniform flow conditions at the impeller discharge. Thus, the friction losses in most vaneless diffuser designs are considerable and result from the (usually) large ratio of wetted surface to flow area. The diffuser efficiency can be improved by lower values for  $\xi$  (provided other design and flow variables remain unchanged) and these lower values for  $\xi$  can result from lower values of  $\frac{r_T}{h_T}$ , which means, for example, larger compressor flow rates for a given impeller tip radius.

A general conclusion resulting from the first group of numerical examples is that heat transfer from the fluid has the opposite effect of friction on pressure rise in vaneless diffusers and is therefore to be desired. Heat transfer to the fluid, on the other hand, can be expected to have the same effect as friction and is therefore to be avoided.

### Effects of Diffuser Wall Spacing

The second group of numerical examples shows the effects of passage height  $h$  (that is, spacing of the diffuser walls normal to the mean surface of revolution) on the flow in vaneless diffusers. The losses in a vaneless diffuser should increase with the velocity squared, with the ratio of wetted perimeter (at each radius) to diffuser wall spacing (that is, with the ratio of friction area to flow area), and with the length of the flow path in the vaneless diffuser. For a given compressor flow rate the square of the velocity and the ratio of wetted perimeter to diffuser wall spacing increases as the diffuser wall spacing  $h$  is decreased, but the length of the flow path decreases. The object of the second group of numerical examples is to determine the relative magnitudes of these opposing effects on the losses in vaneless diffusers, and to determine the optimum wall spacing  $h$ , if such an optimum exists.

Diffuser design. - As for the first group of numerical examples the diffusers of the second group were designed for constant flow area ( $H = R^{-1}$ ) but with the diffuser wall spacing  $h_T$  at the impeller discharge (diffuser inlet), and therefore throughout the diffuser, varying (among examples) over a wide range. The values of  $h_T$  were selected for the eight numerical examples of the second group such that the friction parameter  $\zeta$  varied from 0.010 to 0.038 in seven increments of 0.004. ( $\zeta$  varies inversely with  $h_T$ , equation (13d).) The friction coefficient was assumed to be constant, that is independent of diffuser wall spacing, and therefore the possibility of separated flow for large spacing of the diffuser walls was not considered. Heat-transfer effects were not considered. The example for  $\zeta = 0.030$  was the same as that in the first group of numerical examples with friction but no heat transfer.

Inlet conditions. - For the second group of numerical examples the diffuser inlet conditions varied with the diffuser wall spacing because for a constant compressor flow rate  $W$  the compressor flow coefficient  $\varphi$  (equation (C11), appendix C) varies inversely with the passage height  $h_T$  at the impeller tip. (Note that the blade height at the impeller tip is also assumed to vary with  $h_T$  and this variation is assumed to have no effect on the impeller efficiency, and so forth.) For the selected variation in  $h_T$  the flow coefficient varies from 0.25 to 0.95 in seven increments of 0.10. The remaining design and operating conditions of the impeller are the same as for the first group of examples. Thus,

Impeller tip Mach number,  $M_T$  . . . . . 1.5  
 Impeller slip factor,  $\mu$  . . . . . 0.9  
 Impeller polytropic efficiency,  $\eta$  . . . . . 0.9  
 Compressor stagnation inlet temperature,  $T_o$ ,  $^{\circ}R$  . . . . . 520

The flow conditions at the diffuser inlet were estimated (by methods given in appendix C) from the impeller design and operating conditions and are given in the following table:

Example	$\zeta$	$\varphi$	$P_1$	$M_1^2$	$(\tan \beta)_1$	$\left(\frac{T_t}{T_o}\right)_1$
a	0.010	0.25	3.174	1.272	11.879	941
b	.014	.35	3.157	1.283	8.453	941
c	.018	.45	3.133	1.298	6.541	941
d	.022	.55	3.103	1.317	5.317	941
e	.026	.65	3.066	1.341	4.462	941
f	.030	.75	3.022	1.370	3.829	941
g	.034	.85	2.970	1.406	3.339	941
h	.038	.95	2.909	1.448	2.945	941

Results. - The results of the second group of eight numerical examples are given in figure 9. All results are based on the assumption that as the diffuser wall spacing increases, that is as  $\varphi$  decreases, the friction coefficient remains constant and flow separation does not occur on the diffuser walls. In figure 9(a) is shown the change in  $M^2$  with  $R$  for the eight examples. The effect of decreasing  $\varphi$  (that is, of increasing  $h_T$ ) is to decrease  $M^2$  at each value of  $R$ . This decrease in  $M^2$  results primarily from the decrease in  $q_m$  resulting from the increased flow area that occurs when  $h_T$  is increased.

In figure 9(b) is shown the change in  $P$  with  $R$  for various values of  $\varphi$ . The effect of decreasing  $\varphi$  is to increase  $P$  because  $M^2$  is decreased (fig. 9(a)).

The change in  $\beta$  with  $R$  for various values of  $\varphi$  is shown in figure 9(c). As  $\varphi$  is decreased the velocity component  $q_m$  decreases so that the flow direction  $\beta$  increases as shown. As  $\varphi$  approaches zero,  $\beta$  approaches  $90^\circ$  for all values of  $R$ .

In figure 9(d) is shown the flow path in the vaneless diffuser for the various values of  $\varphi$ . The effect of increasing  $\varphi$  is to decrease the length of the flow path because  $\beta$  is reduced (fig. 9(c)).

The change in polytropic efficiency  $\eta$  with  $R$  for the various values of  $\varphi$  is shown in figure 9(e). The effect of decreasing  $\varphi$  is to increase  $\eta$  at the larger values of  $R$ . As the value of  $\varphi$  decreases the length of the flow path increases (fig. 9(d)), which should increase the diffuser losses, but  $M^2$  (fig. 9(a)) and the friction parameter  $\xi$  decrease, which should decrease the losses. At  $\varphi$  equal to zero  $\beta$  is  $90^\circ$ , or  $\cos \beta$  is zero, and  $\xi$  is zero so that the ratio  $\xi/\cos \beta$  contained in the expression for  $\eta$  (equation (20a)) becomes indeterminate. However, extrapolation of the results in figure 9(f) indicates that  $\eta$  has its peak value for  $\varphi$  equal to zero; and thus, if separation does not occur and if the friction coefficient  $c_f$  is unaffected by the diffuser wall spacing, the diffuser efficiency is always improved (slightly, see fig. 9(f)) by spacing the diffuser walls farther apart. Furthermore, if the diffuser walls are spaced farther apart and the compressor flow rate is increased proportionately so that  $\varphi$  remains unchanged, the diffuser efficiency should be improved markedly because the ratio of wetted surface to flow area is decreased without increasing the length of the flow path in the diffuser and without introducing the risk of boundary-layer separation, which must otherwise be expected if the diffuser walls are spaced far apart. Thus, as also concluded from the first group of numerical examples, the diffuser efficiency can be improved by increased compressor flow rates for a given impeller tip radius so that the diffuser walls can be spaced farther apart without resulting in boundary-layer separation or increasing the length of the flow path.

In figure 9(f) is shown the effect of  $\varphi$  on the diffuser efficiency  $(\eta_D)_2$ . As expected from figure 9(e),  $(\eta_D)_2$  increases as  $\varphi$  decreases, but the rate of increase is less for the smaller values of  $\varphi$  and in no case are large gains in efficiency to be realized by decreasing  $\varphi$ , that is, increasing the diffuser wall spacing. Thus, unless the flow rate is increased proportionately so that  $\varphi$  remains constant, very wide spacing of the diffuser walls is not recommended because of (only) a small gain in efficiency and a great risk of boundary-layer separation.

#### A Vaneless Diffuser Design Problem

The third part of the section on numerical examples is a sample vaneless diffuser design problem. The design variables in a vaneless diffuser are

$$H = H(R)$$

and

$$\alpha = \alpha(R)$$

In this sample design problem  $\alpha(R)$  will be specified (constant and equal to  $90^\circ$ ) and the design problem will be to determine  $H(R)$  for a prescribed variation in  $q_m$ .

For purposes of demonstrating the design method it is assumed that the deceleration of  $q_m$  is the criterion for boundary-layer separation in a vaneless diffuser and that the criterion is that given in reference 5, page 159, so that a safe rate of deceleration is

$$\frac{\delta}{q_m} \frac{dq_m}{dr} = -0.05$$

where  $\delta$  is proportional to the boundary-layer thickness. For purposes of this design example it is assumed that  $\delta$  is equal to  $h/2$ , which is the effective thickness of a fully developed boundary layer in the vaneless diffuser. Thus,

$$\frac{(H/2)}{q_m} \frac{dq_m}{dR} \left( \frac{h_T}{r_T} \right) = -0.05$$

or

$$\frac{1}{q} \frac{dq_m}{dR} = \frac{-1}{H}$$

if  $r_T/h_T$  is equal to 10. Because of the assumptions involved this specified variation in  $\frac{dq_m}{dR}$  with  $H$  may have no practical significance with regard to vaneless diffuser performance and has been selected only to demonstrate an application of the design method. It should be pointed out that design variations in  $H$  affect primarily the velocity component  $q_m$  and through this component the flow direction  $\beta$ .

Inlet conditions. - The impeller design and operating conditions are the same as for the first group of numerical examples and so the diffuser inlet conditions are the same

$$P_1 = 3.022$$

$$M_1^2 = 1.370$$

$$(T_t)_1 = 941^\circ \text{ R}$$

$$(\tan \beta)_1 = 3.829$$

Diffuser design. - The variation in  $H$  with  $R$  is to be determined. Heat-transfer effects are neglected, and the value of the friction parameter  $\xi$  is the same as for the first group of numerical examples (0.030).

Results. - The results of the design problem are given in figure 10. In figure 10(a) is shown the variations in  $H$ ,  $\frac{1}{q_m} \frac{dq_m}{dR}$ ,  $M^2$ ,  $P$ ,  $\beta$ , and  $\eta$  with radius  $R$ . As specified,  $\frac{1}{q_m} \frac{dq_m}{dR}$  is equal to  $-H^{-1}$ . In order to accomplish this variation,  $H$  at first decreases with increasing  $R$  and then increases to approximately its initial value at  $R$  equal to 2.0. At the larger values of  $R$  this variation in  $H$  results in somewhat wider spacing of the diffuser walls than existed in the previous numerical examples where the wall spacing decreased continuously with increasing  $R$  in order to maintain a constant flow area normal to  $q_m$ . As a result of this wider spacing of the diffuser walls the values of  $\eta$  are somewhat higher (in keeping with the results of the second group of numerical examples) than for the previous examples with the same values of  $\phi$  and  $\xi$ . The variation in  $\beta$  with  $R$  was slightly more than  $3^\circ$  so that the flow path (fig. 10(b)) is approximately a logarithmic spiral.

## SUMMARY OF RESULTS AND CONCLUSIONS

An analysis method and a design method have been developed for one-dimensional, compressible flow with friction, heat transfer, and arbitrary area change in vaneless diffusers with arbitrary profiles in the axial-radial plane. The effects of mixing losses due to nonuniform flow conditions at the impeller discharge are not considered. In the analysis method the variation in fluid properties, including the velocity and flow direction, can be determined as a function of radius for a prescribed variation in diffuser wall spacing with radius. In the design method the variation in diffuser wall spacing and all fluid properties except one can be determined as a function of radius for a prescribed variation in the one fluid property. For efficient diffuser designs the selection of the one fluid property and its optimum prescribed variation will depend on viscous flow effects that are considered in boundary-layer studies but are not investigated in this report.

Three groups of numerical examples are presented in which the effects of friction, heat transfer, and diffuser wall spacing are investigated; and a sample design problem is presented. As a result of these examples it is concluded that:

1. Heat transfer from the fluid has the opposite effect of friction on pressure rise in vaneless diffusers and is therefore to be desired. Conversely, heat transfer to the fluid has the same effect as friction and is therefore to be avoided.
2. If the friction coefficient is unaffected by the diffuser wall spacing, and if flow separation does not occur, the diffuser efficiency is improved slightly (for a given compressor flow rate) by spacing the diffuser walls farther apart.
3. Even with relatively low friction coefficients and neglecting mixing losses at the impeller tip, the friction losses in most vaneless diffuser designs are considerable, as indicated by computed diffuser efficiencies in the low 80's, and these losses result from the usually large ratio of wetted surface to flow area in vaneless diffusers.
4. Diffuser efficiencies can be improved by increased compressor flow rates for a given impeller tip radius so that the diffuser walls can be spaced farther apart (thus, reducing the ratio of wetted surface to flow area) without increasing the length of the flow path in the diffuser.
5. In the presence of even small heat-transfer effects the usual definition of diffuser efficiency, which definition neglects corrections for heat transfer, is not a measure of the diffuser losses.

Lewis Flight Propulsion Laboratory  
National Advisory Committee for Aeronautics  
Cleveland, Ohio, September 11, 1951

## APPENDIX A

## SYMBOLS

The following symbols are used in this report:

$a_T$	annulus flow area at impeller tip, equation (C12)
$c$	local speed of sound
$c_f$	skin-friction coefficient, equation (B2)
$c_o$	stagnation speed of sound upstream of impeller
$c_p$	specific heat at constant pressure
$c_t$	local stagnation speed of sound
$g$	acceleration due to gravity
$H$	effective passage height, or diffuser wall spacing, ratio, $h/h_T$
$h$	effective passage height, or diffuser wall spacing
$h'$	coefficient of heat transfer, equation (11a)
$I_1, I_2, I_3, I_4$	influence coefficients, equation (19)
$i$	enthalpy
$J$	mechanical equivalent of heat
$M$	local Mach number, equation (5)
$M_T$	impeller tip Mach number, equation (C3)
$n$	polytropic exponent, equation (C6)
$P$	pressure ratio, $p/p_o$
$p$	static (stream) pressure
$p_o$	stagnation pressure upstream of impeller
$dQ$	heat transfer rate from the fluid

$q$	velocity
$q_m$	velocity component in meridional, or axial-radial, plane, equation (3)
$q_r, q_\theta, q_z$	velocity components in r-, $\theta$ -, and z-directions, respectively
$R$	radius ratio, $r/r_T$
$R^*$	perfect gas constant
$r, \theta, z$	cylindrical coordinates, $\theta$ considered positive in counterclockwise direction when $r\theta$ -plane is viewed from negative z-direction
$T$	static (stream) temperature
$T_0$	stagnation temperature upstream of impeller
$T_t$	local stagnation, or total, temperature
$T_w$	diffuser wall temperature
$t$	time
$W$	compressor flow rate
$X$	dependent variable
$\alpha$	slope of center line between diffuser walls in meridional, or axial-radial plane, equation (2)
$\beta$	flow direction on mean surface of revolution between diffuser walls, equation (4a)
$\gamma$	ratio of specific heats
$\Delta$	small finite increment
$\xi$	friction parameter, equation (13d)
$\eta$	polytropic, or small-stage, efficiency, equation (E1)
$(\eta_D)_R$	diffuser adiabatic efficiency based upon change in flow conditions for change in radii from 1.0 to $R$ , equation (E5)

$\mu$	impeller slip factor
$\rho$	static (stream) weight density
$\rho_0$	stagnation density upstream of impeller
$\rho_t$	local stagnation density
$\tau$	shear stress due to skin friction
$\varphi$	compressor flow coefficient, equation (C11)
$\omega$	angular velocity of impeller

## Subscripts:

a	actual
i	ideal
R	value at R
T	impeller tip
1, 2	value at R equal to 1.0 or 2.0

## APPENDIX B

## EQUILIBRIUM EQUATIONS

Meridional and tangential equilibrium equations are developed for a fluid particle on the mean surface of revolution in a vaneless diffuser.

Meridional equilibrium. - The equation for meridional equilibrium of a fluid particle (fig. 6) in the direction of  $q_m$  on the mean surface of revolution is obtained from a balance of the pressure and shear forces with the force required for acceleration.

The differential pressure forces (opposed to the direction of  $q_m$ ) are equal to the differential change of end forces on the particle minus the component of the differential side forces on the particle in the direction of  $q_m$ ,

$$\text{Differential pressure forces} = \frac{d(p r d\theta) dr}{dr} - \frac{p d(h r d\theta) dr}{dr} \quad (B1)$$

where the component of the differential side forces in the direction of  $q_m$  (last term in equation (B1)) is equal to the pressure  $p$  multiplied by the projected area (in the direction of  $q_m$ ) of the side surfaces of the particle (fig. 6).

The differential shear stress  $\tau$  on a diffuser wall is opposed to the direction of  $q$  and is given by

$$\tau = c_f \frac{\rho q^2}{2g} \quad (B2)$$

where  $c_f$  is the skin friction coefficient. The differential shear forces in the meridional direction on the fluid particle in figure 6 are opposed to the direction of  $q_m$  and act on both walls of the diffuser. From equation (B2),

$$\begin{aligned} \text{Differential shear forces} &= 2\tau \cos \beta \frac{r d\theta dr}{\sin \alpha} \\ &= c_f \frac{\rho q^2}{g} \cos \beta \frac{r d\theta dr}{\sin \alpha} \quad (B3) \end{aligned}$$

The acceleration of the fluid particle in the direction opposed to  $q_m$  is made up of: (1) the component of the centripetal acceleration  $\frac{q_\theta^2}{r} \sin \alpha$ , and (2) the negative of the acceleration  $\frac{dq_m}{dt}$ . But,

$$\frac{dq_m}{dt} = \frac{dq_m}{dr} \frac{dr}{dt} = q_m \frac{dq_m}{dr} \sin \alpha$$

so that the differential force required for acceleration of the fluid particle in figure 6 becomes

$$\left( \begin{array}{l} \text{Differential force required} \\ \text{for acceleration in direc-} \\ \text{tion opposed to } q_m \end{array} \right) = \frac{\rho}{g} \frac{hr}{\sin \alpha} \frac{d\theta}{dr} \left( \frac{q_\theta^2}{r} \sin \alpha - q_m \frac{dq_m}{dr} \sin \alpha \right) \quad (B4)$$

The sum of the differential pressure forces and shear forces must equal the force required for acceleration so that from equations (B1), (B3), and (B4)

$$\frac{g}{\rho} \frac{dp}{dr} + \frac{c_f q^2 \cos \beta}{h \sin \alpha} = \frac{q_\theta^2}{r} - q_m \frac{dq_m}{dr} \quad (8)$$

Equation (8) is the equation for meridional equilibrium of a fluid particle on the mean surface of revolution in a vaneless diffuser.

Tangential equilibrium. - The equation for equilibrium of a fluid particle (fig. 6) in the tangential direction on the mean surface of revolution is obtained from a balance of the shear forces with the force required for acceleration.

The differential shear forces in the tangential direction on the fluid particle in figure 6 are opposed to the direction of  $q_\theta$  and act on both walls of the diffuser. From equation (B2),

$$\begin{aligned} \text{Differential shear forces} &= 2\tau \sin \beta \frac{r}{\sin \alpha} \frac{d\theta}{dr} \\ &= c_f \frac{\rho q^2}{g} \sin \beta \frac{r}{\sin \alpha} \frac{d\theta}{dr} \end{aligned} \quad (B5)$$

The tangential acceleration of the fluid particle opposed to the direction of  $q_\theta$  is made up of: (1) the negative of the tangential acceleration  $r \frac{d}{dt} \left( \frac{q_\theta}{r} \right)$ , and (2) the negative of the Coriolis acceleration  $2q_m q_\theta \frac{\sin \alpha}{r}$ . But,

$$\begin{aligned}
 \frac{d}{dt} \left( \frac{q_\theta}{r} \right) &= \frac{1}{r} \frac{dq_\theta}{dt} - \frac{q_\theta}{r^2} \frac{dr}{dt} \\
 &= \frac{1}{r} \frac{dq_\theta}{dr} \frac{dr}{dt} - \frac{q_\theta}{r^2} \frac{dr}{dt} \\
 &= \frac{q_m \sin \alpha}{r} \left( \frac{dq_\theta}{dr} - \frac{q_\theta}{r} \right)
 \end{aligned}$$

so that the differential force required for acceleration of the fluid particle in figure 6 becomes

$$\left( \begin{array}{l} \text{Differential force required} \\ \text{for acceleration in direc-} \\ \text{tion opposed to } q_\theta \end{array} \right) = - \frac{\rho}{g} \frac{hr}{\sin \alpha} \frac{d\theta}{dr} \frac{dr}{dt} \left( q_m \frac{dq_\theta}{dr} \sin \alpha + \frac{q_m q_\theta \sin \alpha}{r} \right) \quad (B6)$$

The differential shear force must equal the differential force required for acceleration so that from equations (B5) and (B6)

$$- \frac{c_f q^2 \sin \beta}{h \sin \alpha} = q_m \frac{dq_\theta}{dr} + \frac{q_m q_\theta}{r} \quad (9)$$

Equation (9) is the equation for tangential equilibrium of a fluid particle (fig. 6) in the tangential direction on the mean surface of revolution in a vaneless diffuser.

## APPENDIX C

ESTIMATED VALUES OF  $T_t$ ,  $M^2$ ,  $P$ , AND  $\tan \beta$  AT DIFFUSER

## INLET (IMPELLER TIP)

Total temperature. - The total temperature  $(T_t)_1$  at the diffuser inlet, or impeller tip, can be obtained from the steady flow energy equation, where for convenience heat-transfer effects have been considered negligible,

$$Jc_p T_o + \mu \frac{(\omega r_T)^2}{g} = Jc_p T_1 + \frac{(q_m^2 + q_\theta^2)_1}{2g} \quad (C1)$$

where  $\mu$  is the impeller slip factor and  $\omega$  is the angular velocity of the impeller so that  $\mu(\omega r_T)^2/g$  is the impeller work per pound of fluid. But

$$Jc_p = \frac{\gamma R^*}{\gamma - 1}$$

and

$$(q_\theta)_1 = \mu \omega r_T$$

so that dividing equation (C1) by  $Jc_p T_o$

$$\frac{T_1}{T_o} = 1 + \frac{\gamma - 1}{2} \left[ (2\mu - \mu^2) M_T^2 - \frac{(q_m)_1^2}{c_o^2} \right] \quad (C2)$$

where the impeller tip Mach number  $M_T$  is defined by

$$M_T = \frac{\omega r_T}{c_o} \quad (C3)$$

The total temperature  $(T_t)_1$  is given by equation (C2) when  $\frac{(q_m)_1^2}{c_o^2}$  and  $\frac{(q_\theta)_1^2}{c_o^2}$  (equal to  $\mu^2 M_T^2$ ) are equal to zero so that

$$(T_t)_1 = T_o \left[ 1 + (\gamma - 1) \mu M_T^2 \right] \quad (C4)$$

Pressure. - The pressure  $P_1$  at the diffuser inlet is obtained from the temperature ratio (equation (C2)) by

$$\frac{p_1}{p_0} = P_1 = \left( \frac{T_1}{T_0} \right)^{\frac{n}{n-1}} \quad (C5)$$

where the flow in the impeller, which involves viscous losses, is represented by a polytropic process for which the polytropic exponent  $n$  is related to the polytropic efficiency of the impeller  $\eta$  by (reference 8, p. 449, for example)

$$\frac{n}{n-1} = \eta \frac{\gamma}{\gamma-1} \quad (C6)$$

The quantity  $(q_m)_1$  in equation (C2) is unknown but will be determined later from continuity considerations.

In like manner the density  $\rho_1$  is related to the temperature ratio (equation (C2)) by

$$\frac{\rho_1}{\rho_0} = \left( \frac{T_1}{T_0} \right)^{\frac{1}{n-1}} \quad (C7)$$

Mach number. - The local Mach number squared  $(M^2)_1$  at the diffuser inlet is defined by

$$(M^2)_1 = \frac{(q_\theta)_1^2 + (q_m)_1^2}{c^2} = \frac{(q_\theta)_1^2 + (q_m)_1^2}{c_0^2} \frac{T_0}{T_1} \quad (C8)$$

where  $T_0/T_1$  is given by equation (C2), where

$$\frac{(q_\theta)_1}{c_0} = \mu M_T \quad (C9)$$

and where  $\frac{(q_m)_1}{c_0}$  is determined from continuity considerations. From continuity

$$W = 2\pi r_T h_T \rho_1 (q_m)_1$$

or

$$\frac{(q_m)_1}{c_0} = \frac{\varphi}{\rho_1/\rho_0} \quad (C10)$$

where the compressor flow coefficient  $\varphi$  is defined by

$$\varphi = \frac{W}{\rho_o a_T c_o} \quad (C11)$$

in which the annulus area at the impeller tip  $a_T$  is given by

$$a_T = 2\pi r_T h_T \quad (C12)$$

Equations (C7) and (C10) are solved simultaneously for  $\frac{(q_m)_1}{c_o}$  so that equation (C8) can be solved for  $(M_1)^2$ .

Flow direction. - The tangent of the flow direction  $\beta_1$  at the diffuser inlet is defined by

$$(\tan \beta)_1 = \frac{(q_\theta/c_o)_1}{(q_m/c_o)_1} \quad (C13)$$

where  $(q_\theta)_1$  and  $(q_m)_1$  are given by equations (C9) and (C10), respectively.

Thus,  $(T_t)_1$ ,  $P_1$ ,  $M_1^2$ , and  $(\tan \beta)_1$  are estimated by equations (C4), (C5), (C8), and (C13), respectively.

## APPENDIX D

## CONDITION FOR MAXIMUM, OR CHOKE, FLOW IN VANELESS DIFFUSERS

If  $W$  is the flow rate through a vaneless diffuser

$$W = 2\pi r h \rho q_m \quad (D1)$$

where  $\rho$  is related to the stagnation density  $\rho_t$  at a given radius  $r$  by (reference 7, p. 26, for example)

$$\rho = \rho_t \left[ 1 - \frac{\gamma-1}{2} \left( \frac{q_m^2 + q_\theta^2}{c_t^2} \right) \right]^{\frac{1}{\gamma-1}} \quad (D2)$$

(In the presence of heat transfer and friction  $\rho_t$  is a function of radius.) At any given radius as  $q_m$  is increased from low values  $W$  increases until a maximum, or choke, flow occurs. This maximum occurs when

$$\frac{dW}{dq_m} = 0$$

or, from equation (D1),

$$0 = \rho + q_m \frac{d\rho}{dq_m} \quad (D3)$$

but, from equation (D2),

$$\frac{d\rho}{dq_m} = \frac{-\rho}{1 - \frac{\gamma-1}{2} \left( \frac{q_m^2 + q_\theta^2}{c_t^2} \right)} \frac{q_m}{c_t^2} \quad (D4)$$

where from reference 7, page 26, for example

$$1 - \frac{\gamma-1}{2} \left( \frac{q_m^2 + q_\theta^2}{c_t^2} \right) = \frac{T}{T_t}$$

so that equation (D4) becomes

$$\frac{d\rho}{dq_m} = -\rho \frac{q_m}{c} \quad (D5)$$

where

$$c^2 = \frac{T}{T_t} c_t^2$$

After equations (D3) and (D5) are combined

$$q_m = c \tag{D6}$$

so that the maximum, or choke, flow occurs in vaneless diffusers when the meridional component of velocity  $q_m$  is equal to the local speed of sound  $c$ . Expressed in terms of  $M^2$  equation (D6) becomes

$$0 = M^2 - \sec^2 \beta \tag{D7}$$

which is the condition for maximum, or choke, flow in vaneless diffusers.

## APPENDIX E

## SMALL-STAGE EFFICIENCY AND DIFFUSER EFFICIENCY

The small-stage, or polytropic, efficiency  $\eta$  at a given radius  $R$  on the mean surface of revolution in a vaneless diffuser is defined as the ratio of the ideal to the actual differential change in static enthalpy with radius required to accomplish the actual differential change in static pressure with radius

$$\eta = \frac{\left(\frac{di}{dr}\right)_i}{\left(\frac{di}{dr}\right)_a} \quad (\text{E1})$$

where the ideal differential change in static enthalpy with radius  $\left(\frac{di}{dr}\right)_i$  is given by (reference 6, p. 102)

$$\left(\frac{di}{dr}\right)_i = \frac{1}{\rho} \frac{dp}{dr} = R^* T \frac{1}{p} \frac{dp}{dr} \quad (\text{E2})$$

and where the actual differential change in static enthalpy with radius  $\left(\frac{di}{dr}\right)_a$  is by definition

$$\left(\frac{di}{dr}\right)_a = J c_p \frac{dT}{dr} = \frac{\gamma R^*}{\gamma - 1} \frac{dT}{dr} \quad (\text{E3})$$

Equation (E1) is the usual definition of small-stage, or polytropic, efficiency and assumes that heat-transfer effects are negligible. From equations (E1) to (E3) and equation (13e)

$$\eta = \frac{\frac{1}{P} \frac{dP}{dR}}{\frac{\gamma}{\gamma - 1} \frac{1}{T} \frac{dT}{dR}} \quad (\text{E4})$$

which from equations (6a) and (13c) becomes

$$\eta = \frac{\frac{1}{P} \frac{dP}{dR}}{\frac{1}{P} \frac{dP}{dR} + \frac{\gamma}{\gamma - 1} \left(1 + \frac{\gamma - 1}{2} M^2\right) \frac{1}{T_t} \frac{dT_t}{dR} + \frac{\gamma M^2 \xi}{H \cos \beta}} \quad (\text{20a})$$

Equation (20a) gives the small-stage, or polytropic, efficiency in terms of the local pressure differential, the total temperature differential and the parameter  $\zeta$ , which involves the local skin-friction coefficient.

In the absence of heat transfer  $\frac{1}{T_t} \frac{dT_t}{dR}$  equals zero and from equations (13c) and (15c)

$$\frac{1}{P} \frac{dP}{dR} = \frac{\gamma M^2}{M^2 - \sec^2 \beta} \left[ (\gamma M^2 - \tan^2 \beta) \frac{\zeta}{H \cos \beta} - \frac{1}{H} \frac{dH}{dR} - \frac{\sec^2 \beta}{R} \right] - \frac{\gamma M^2 \zeta}{H \cos \beta}$$

so that equation (20a) becomes

$$\eta = 1 - \frac{\zeta (M^2 - \sec^2 \beta)}{\zeta (\gamma M^2 - \tan^2 \beta) - \cos \beta \left( \frac{dH}{dR} + \frac{H \sec^2 \beta}{R} \right)} \quad (20b)$$

Equation (20b) expresses  $\eta$  in terms of the friction parameters  $\zeta$  and the diffuser geometry.

The diffuser efficiency  $(\eta_D)_R$ , which measures the diffuser performance between the diffuser inlet at  $R$  equals 1.0 and a point  $R$  on the mean surface of revolution in the vaneless diffuser, is defined as the ratio of the ideal to the actual static temperature rise required to accomplish the actual static pressure rise between the radii 1.0 and  $R$ .

$$(\eta_D)_R = \frac{(T_R - T_1)_i}{(T_R - T_1)_a} = \frac{\left( \frac{T_R}{T_1} - 1 \right)_i}{\left( \frac{T_R}{T_1} - 1 \right)_a} \quad (E5)$$

where the ideal temperature ratio  $\left( \frac{T_R}{T_1} \right)_i$  is related to the actual static pressure ratio by

$$\left( \frac{T_R}{T_1} \right)_i = \left( \frac{P_R}{P_1} \right)^{\frac{\gamma-1}{\gamma}}$$

so that equation (E5) becomes

$$(\eta_D)_R = \frac{\left(\frac{P_R}{P_1}\right)^{\frac{\gamma-1}{\gamma}} - 1}{\frac{T_R}{T_1} - 1} \quad (E6)$$

Equation (E6) gives  $(\eta_D)_R$  in terms of the known values of  $P$  and  $T$  at the radii 1.0 and  $R$ . If  $R$  approaches 1.0,

$$\left(\frac{P_R}{P_1}\right)^{\frac{\gamma-1}{\gamma}} \rightarrow \left(\frac{P + dP}{P}\right)_1 \rightarrow 1 + \frac{\gamma-1}{\gamma} \left(\frac{dP}{P}\right)_1$$

and

$$\frac{T_R}{T_1} \rightarrow \left(\frac{T + dT}{T}\right)_1 \rightarrow 1 + \left(\frac{dT}{T}\right)_1$$

so that

$$(\eta_D)_1 = \left( \frac{\frac{1}{P} \frac{dP}{dR}}{\frac{\gamma-1}{\gamma} \frac{1}{T} \frac{dT}{dR}} \right)_1$$

which corresponds to the definition for the small-stage efficiency given by equation (E4).

#### REFERENCES

1. Polikovsky, V., and Nevelson, M.: The Performance of a Vaneless Diffuser Fan. NACA TM 1038, 1942.
2. Brown, W. Byron, and Bradshaw, Guy R.: Method of Designing Vaneless Diffusers and Experimental Investigation of Certain Undetermined Parameters. NACA TN 1426, 1947.

3. Shapiro, Ascher H., and Hawthorne, W. R.: The Mechanics and Thermodynamics of Steady One-Dimensional Gas Flow. Jour. Appl. Mech., vol. 14, no. 4, Dec. 1947, pp. A317-A336.
4. Brown, W. Byron: Friction Coefficients in a Vaneless Diffuser. NACA TN 1311, 1947.
5. Prandtl, L.: The Mechanics of Viscous Fluids. Vol. III of Aerodynamic Theory, div. G, sec. 13, W. F. Durand, ed., Julius Springer (Berlin), 1943.
6. Keenan, Joseph H.: Thermodynamics. John Wiley & Sons, Inc. (New York), 1941.
7. Liepmann, Hans Wolfgang, and Puckett, Allen E.: Introduction to Aerodynamics of a Compressible Fluid. John Wiley & Sons, Inc. (New York), 1947.
8. Wislicenus, George F.: Fluid Mechanics of Turbomachinery. McGraw-Hill Book Co., Inc. (New York), 1947.

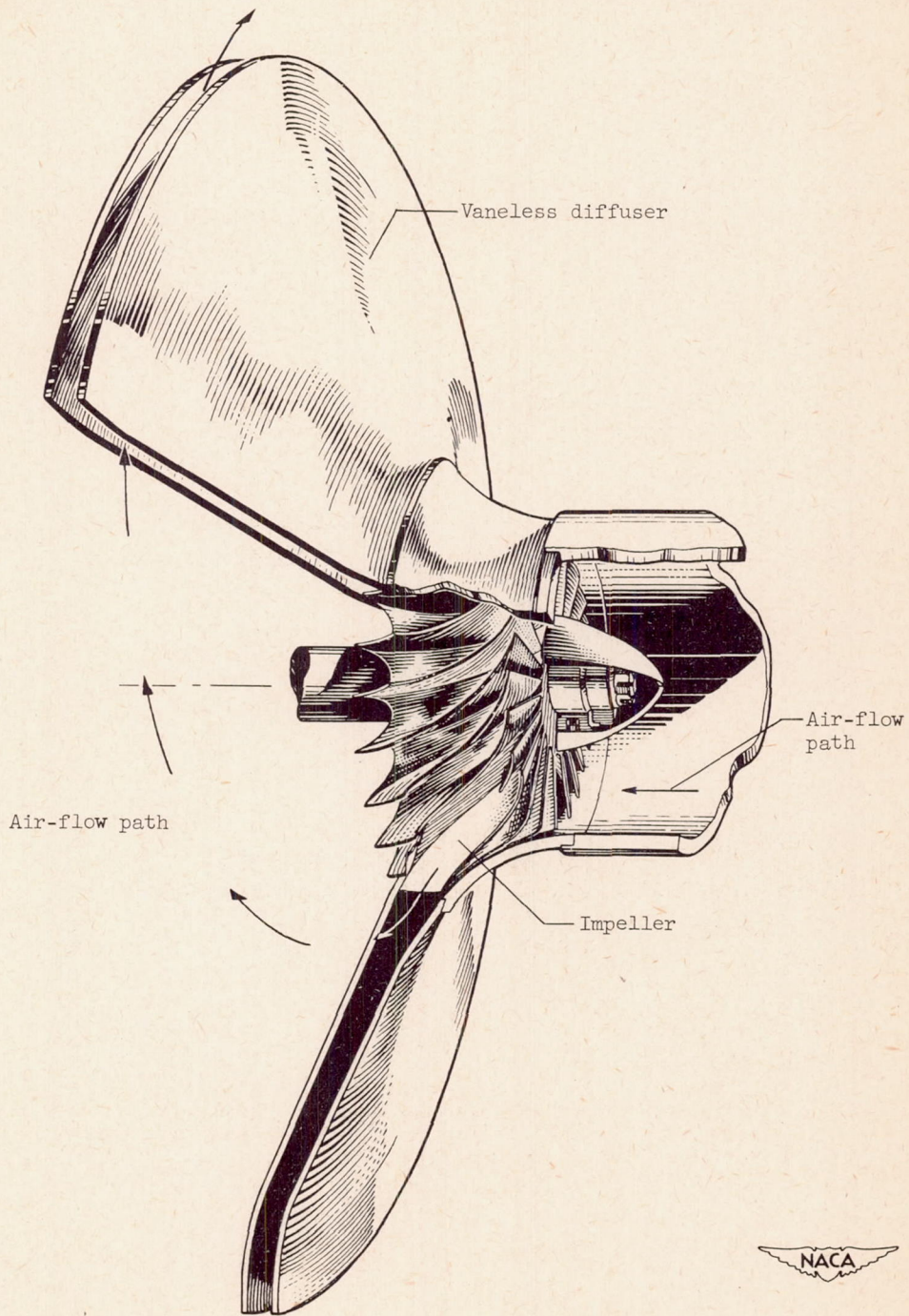


Figure 1. - Assembly of vaneless diffuser with mixed-flow impeller.

2391

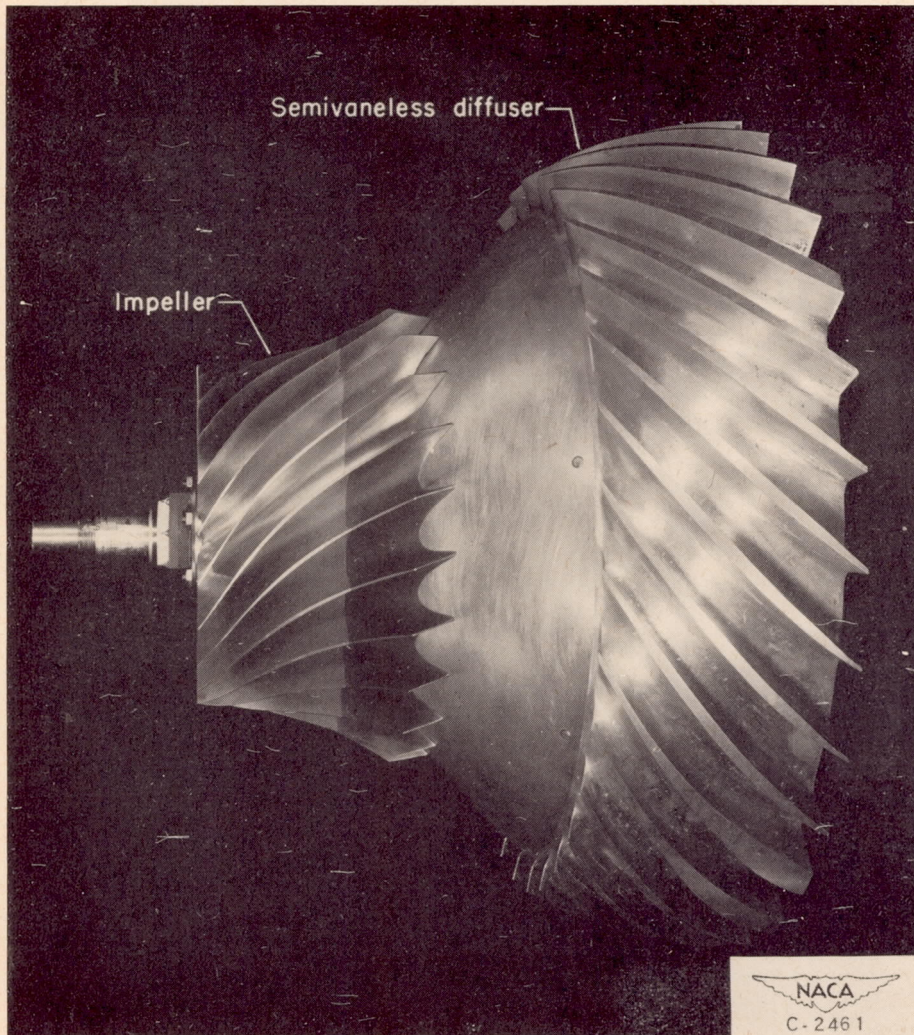


Figure 2. - Mixed-flow impeller and semivaneless diffuser with front shroud removed.

2591

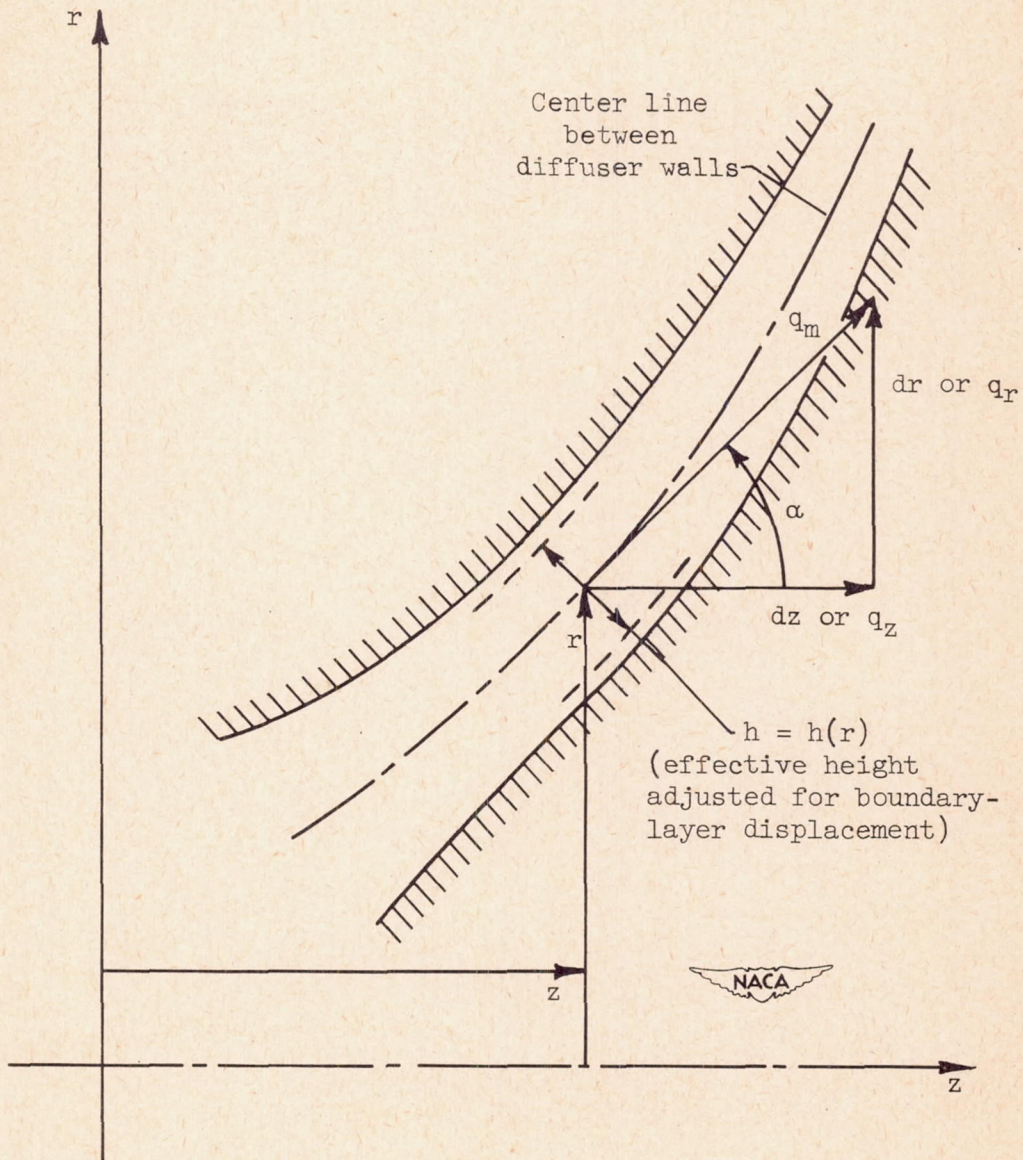


Figure 3. - Diffuser profile, velocity components, and coordinates in meridional, or axial-radial, plane.

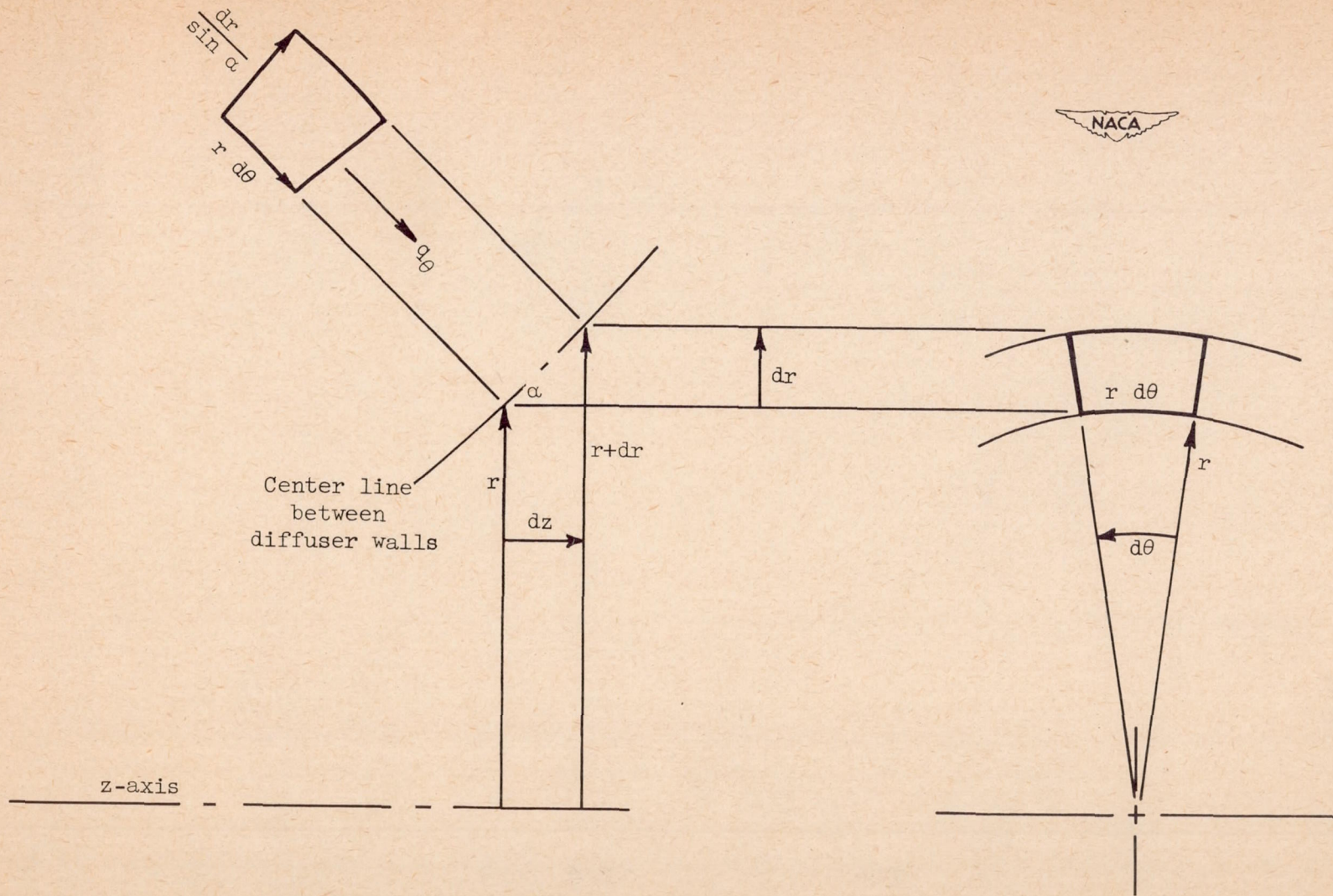
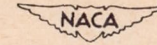


Figure 4. - Fluid particle on surface of revolution generated by center line between diffuser walls.

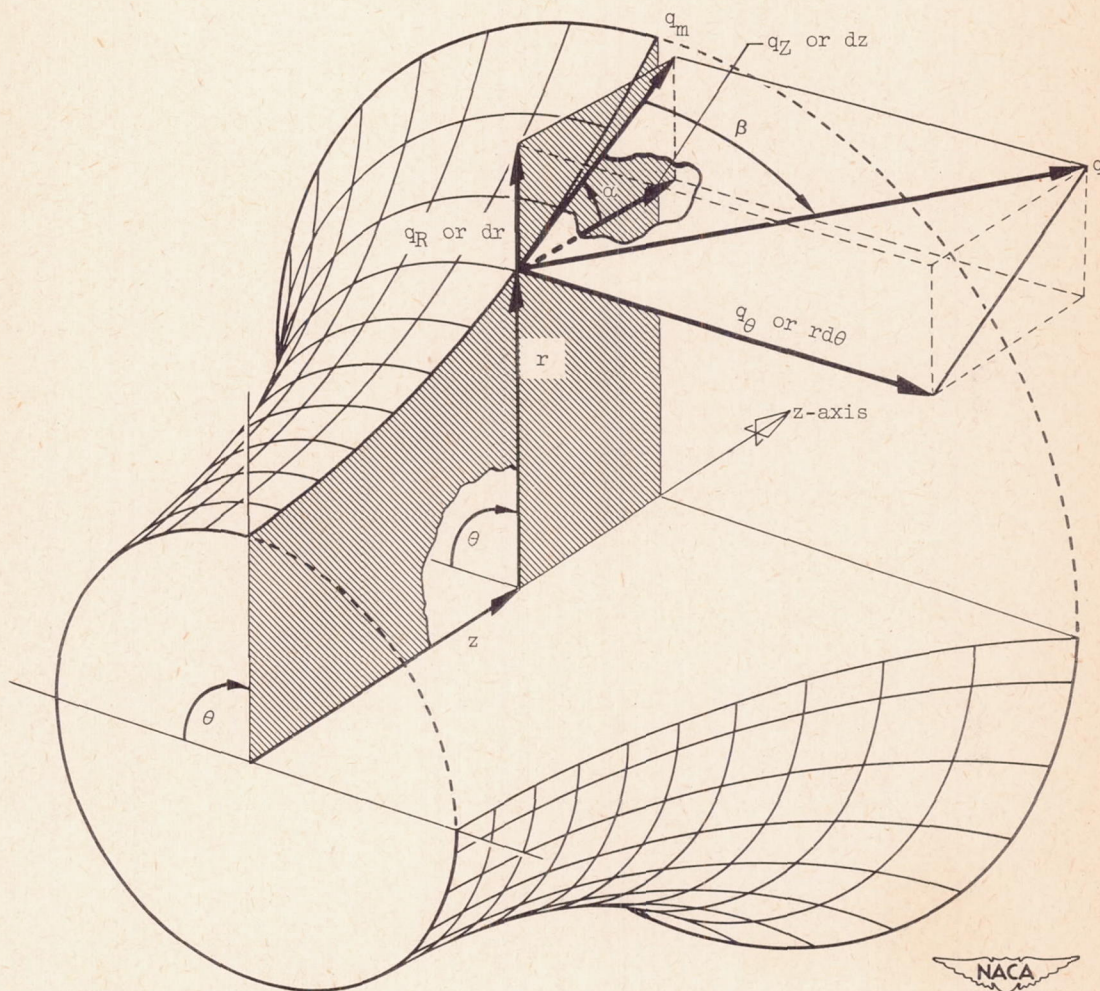
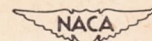


Figure 5. - Mean surface of revolution with coordinates and velocity components.



2391

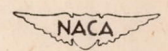
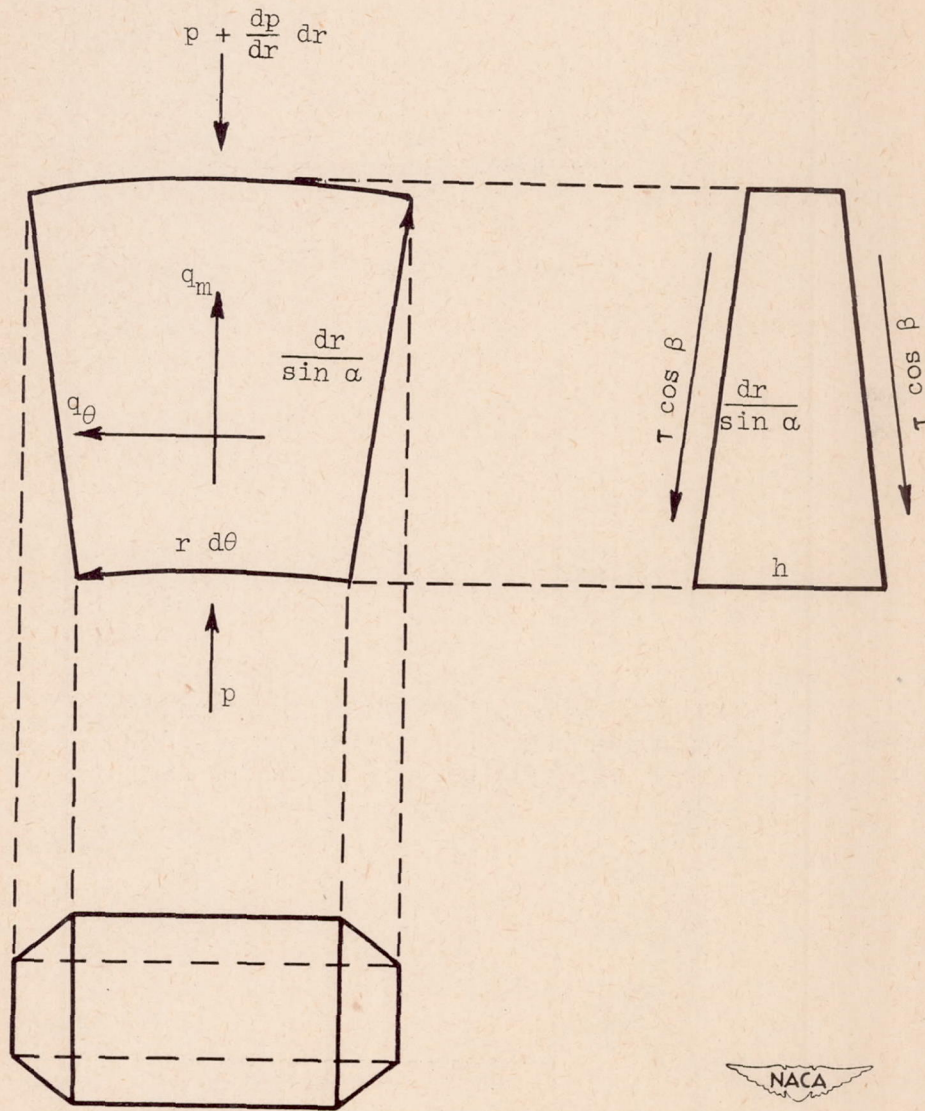


Figure 6. - Fluid particle with pressure and shear forces.

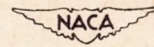
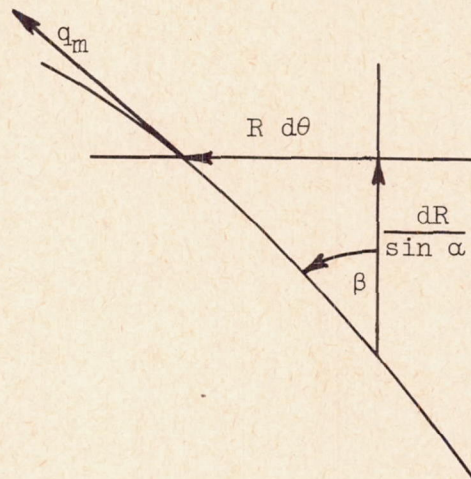
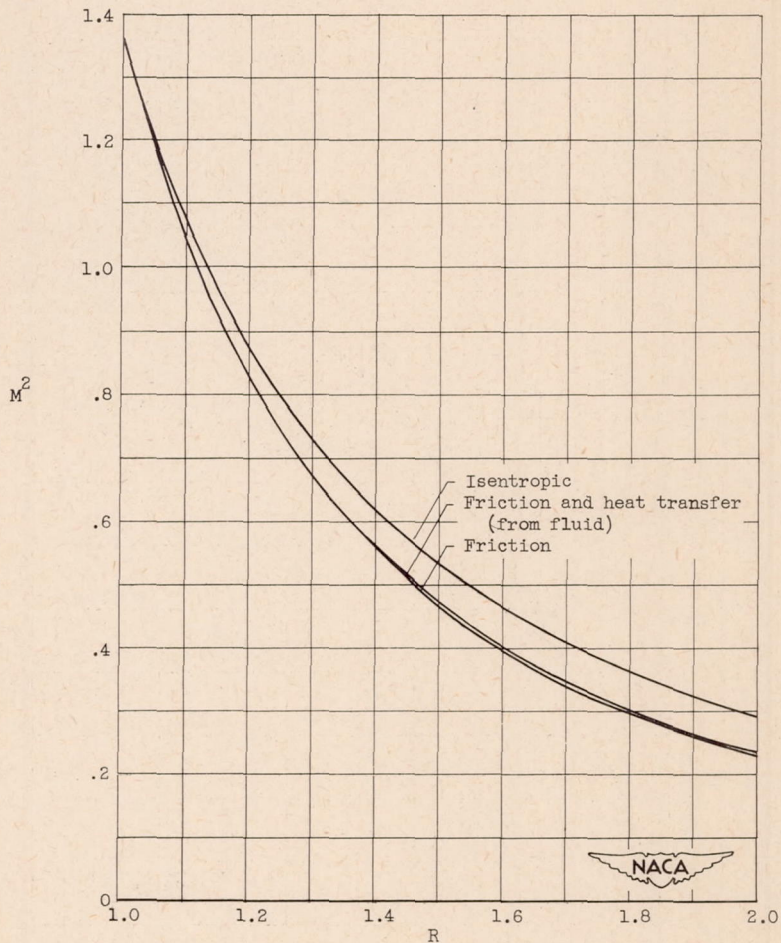


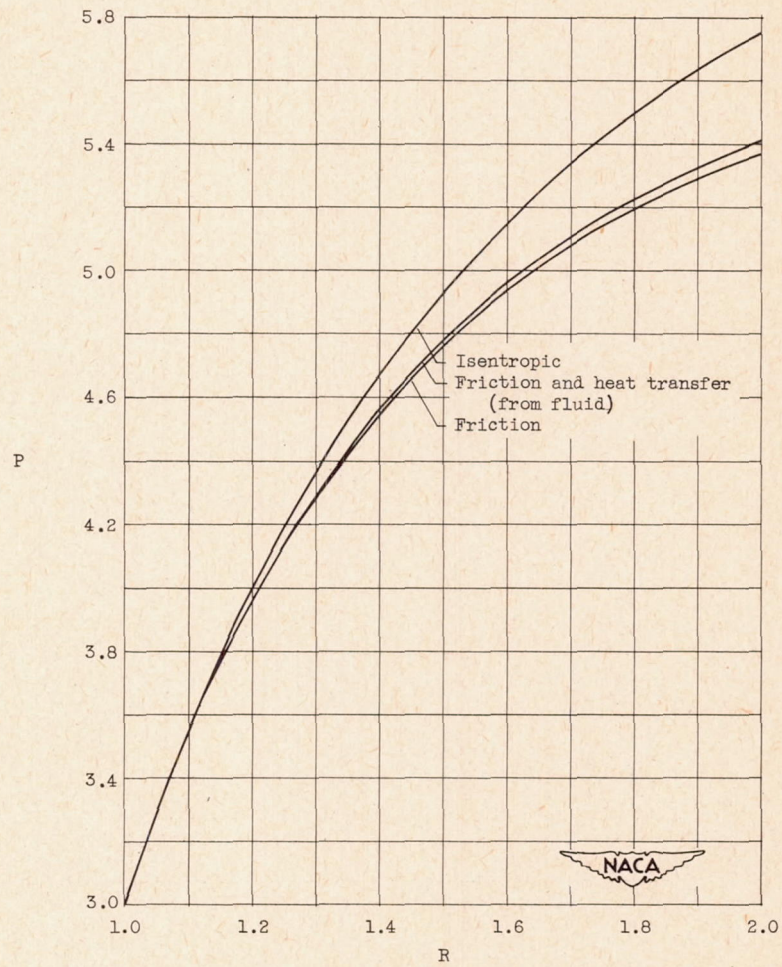
Figure 7. - Developed view of mean surface of revolution (fig. 5) in vicinity of  $R$ , showing relation between  $\beta$ ,  $R d\theta$ , and  $\frac{dR}{\sin \alpha}$ .



(a) Variation in  $M^2$  with radius.

Figure 8. - First group of numerical examples, showing effects of friction and heat transfer.

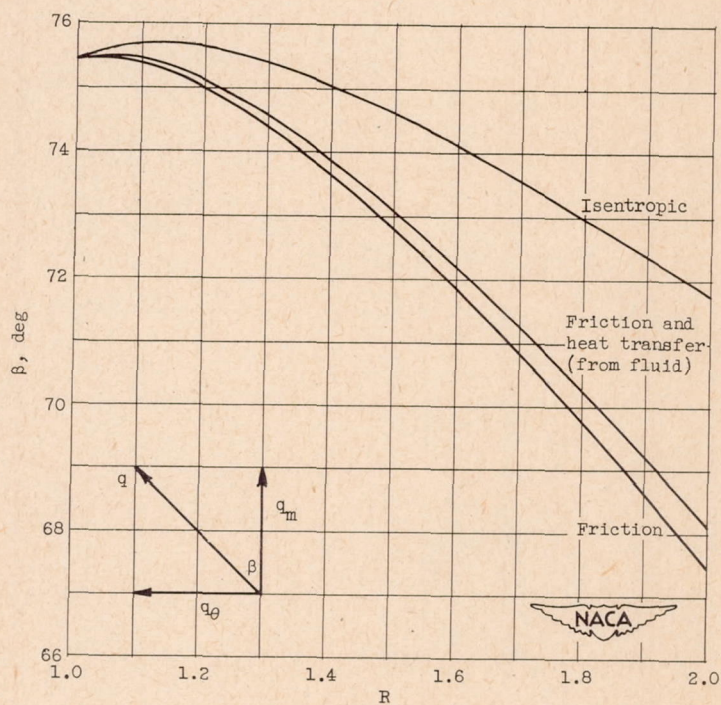
2391



(b) Variation in pressure ratio with radius.

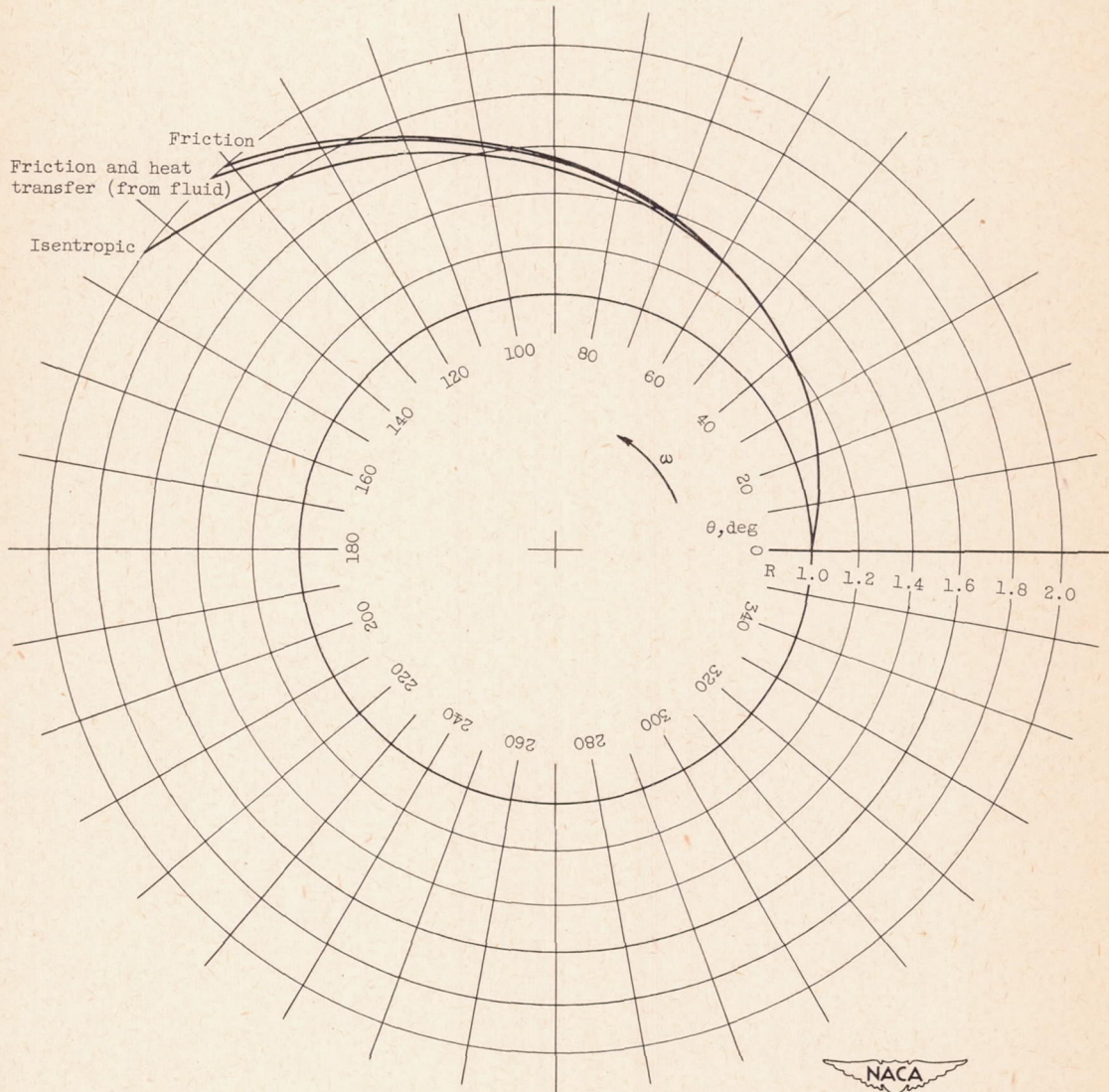
Figure 8. - Continued. First group of numerical examples, showing effects of friction and heat transfer.

2391



(c) Variation in flow direction with radius.

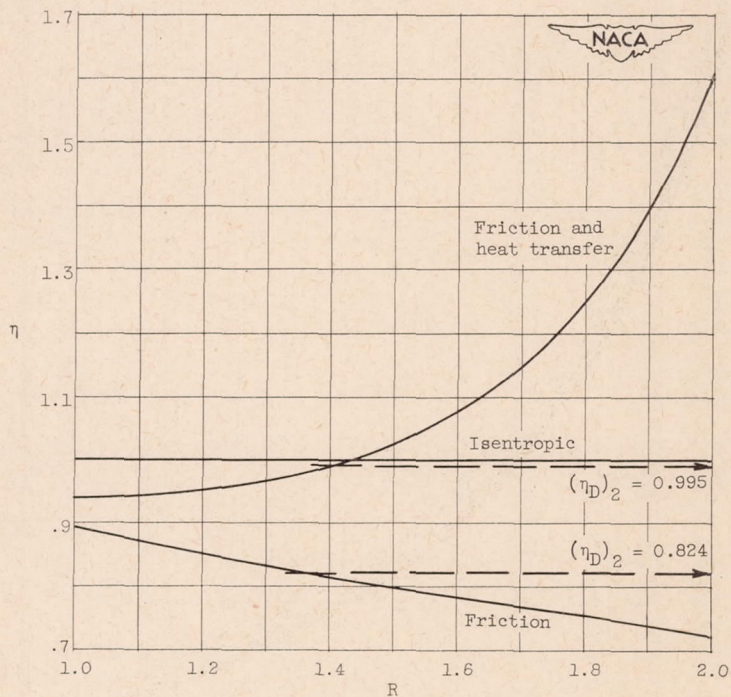
Figure 8. - Continued. First group of numerical examples, showing effects of friction and heat transfer.



(d) Flow path for  $\sin \alpha = 1.0$ .

Figure 8. - Continued. First group of numerical examples, showing effects of friction and heat transfer.

2391



(e) Variation in polytropic, or small-stage, efficiency with radius.

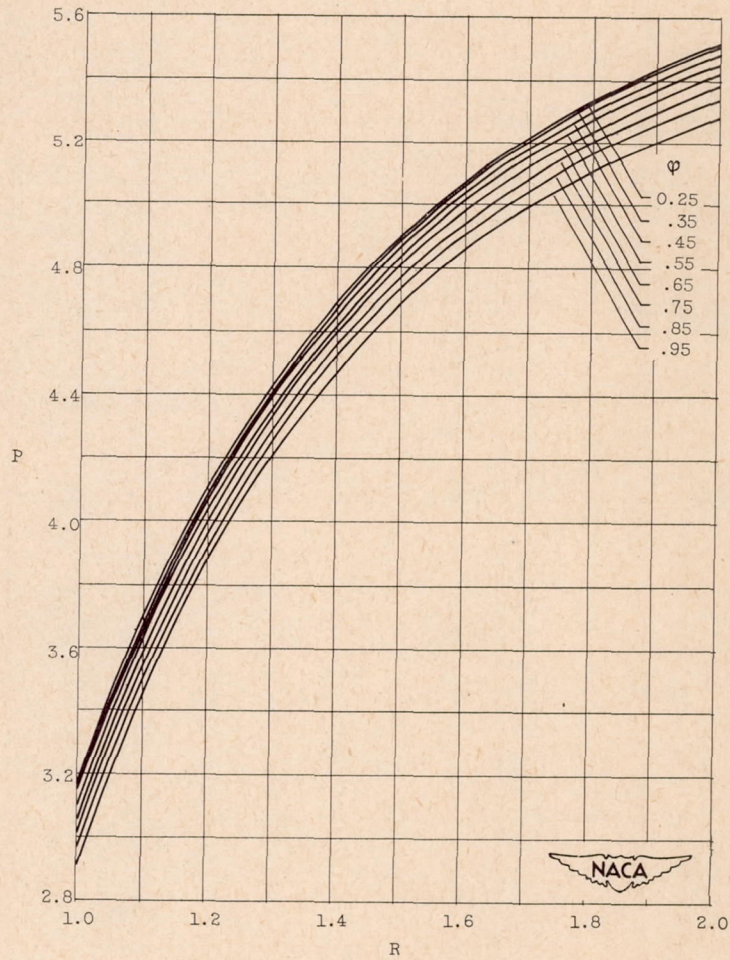
Figure 8. - Concluded. First group of numerical examples, showing effects of friction and heat transfer.



(a) Variation in  $M^2$  with radius.

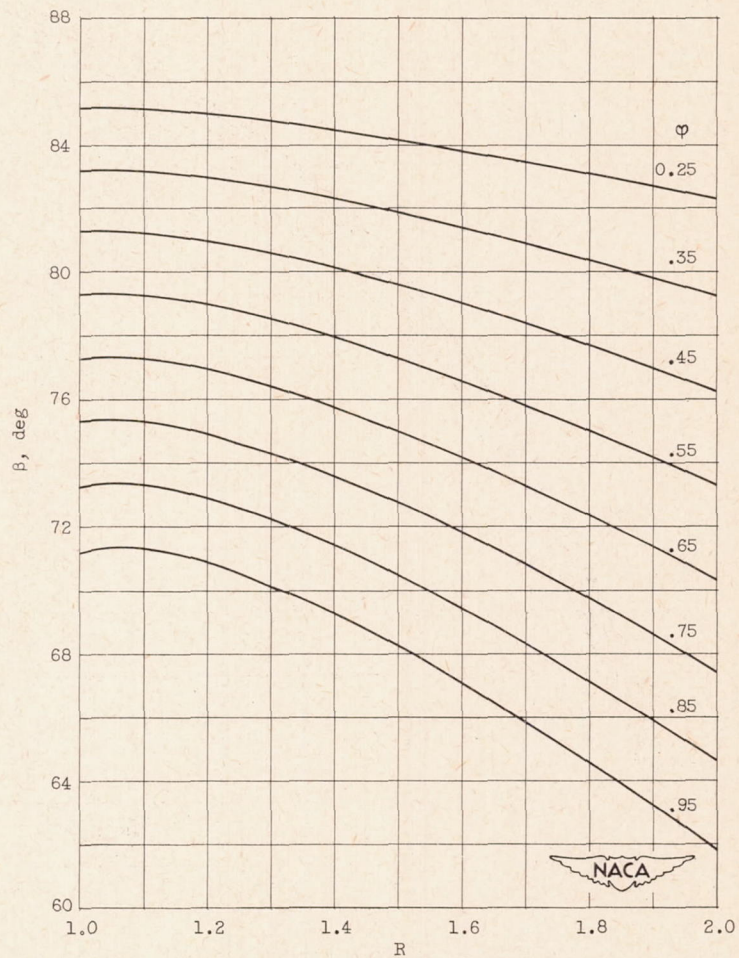
Figure 9. - Second group of numerical examples, showing effect of diffuser wall spacing as affected by changes in compressor flow coefficient  $\phi$ .

2391



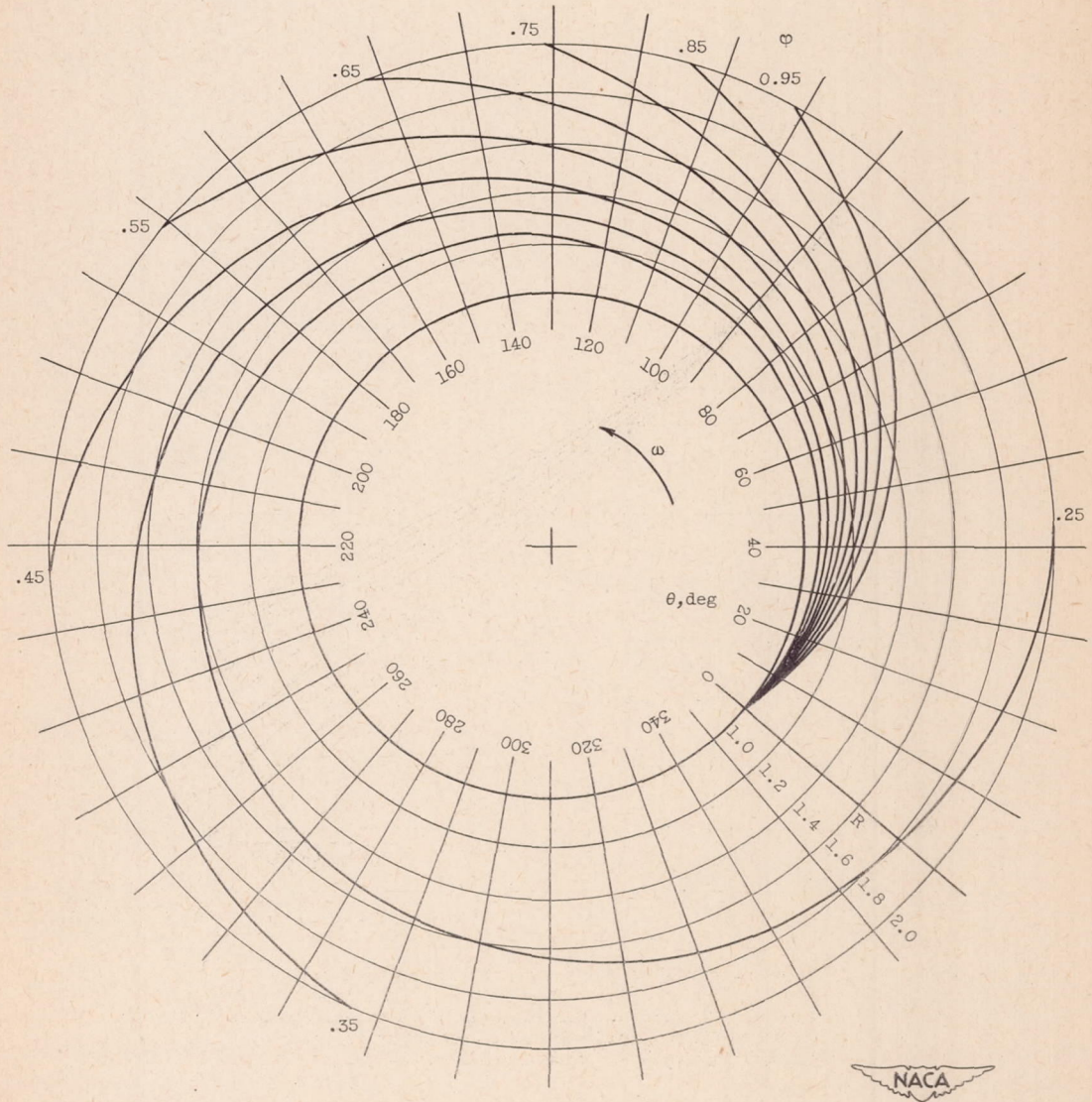
(b) Variation in static pressure ratio with radius.

Figure 9. - Continued. Second group of numerical examples, showing effect of diffuser wall spacing as affected by changes in compressor flow coefficient  $\phi$ .



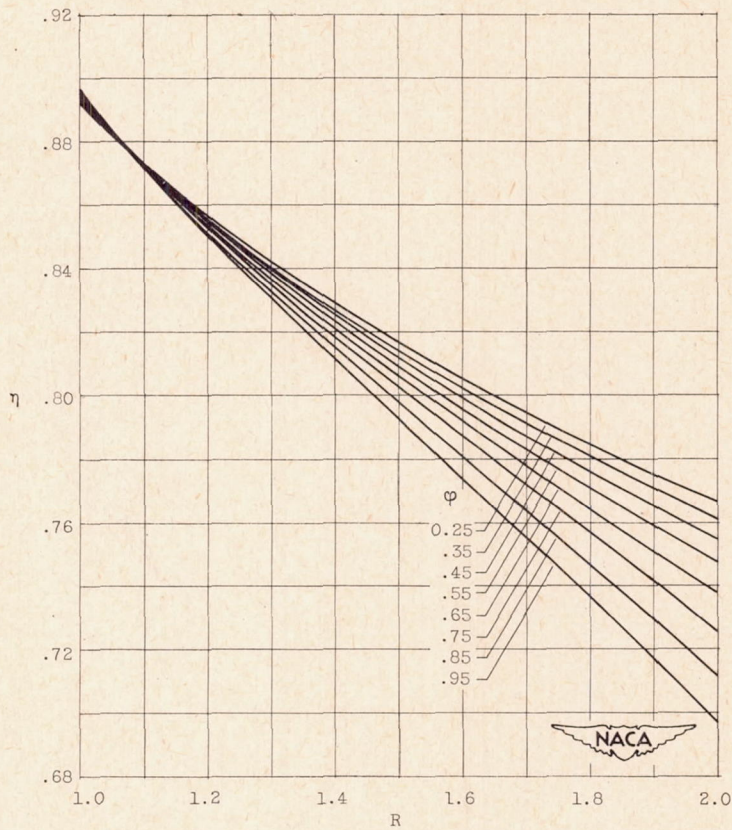
(c) Variation in flow direction with radius.

Figure 9. - Continued. Second group of numerical examples, showing effect of diffuser wall spacing as affected by changes in compressor flow coefficient  $\phi$ .



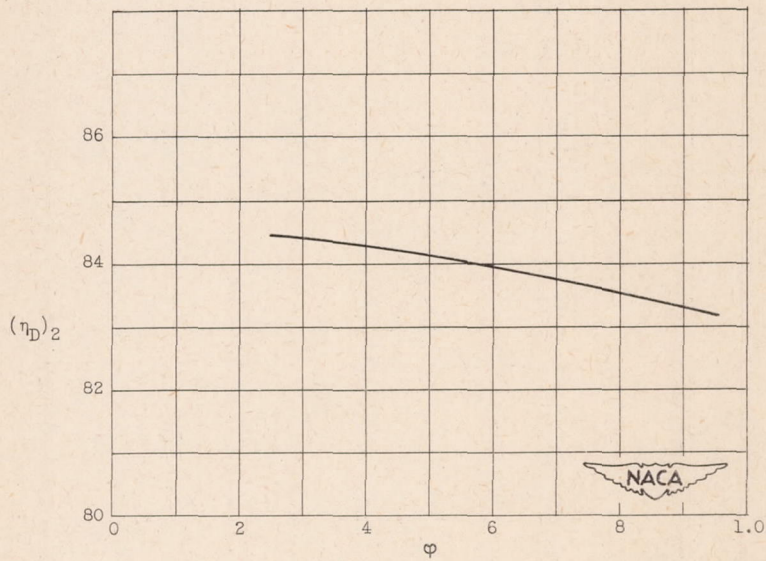
(d) Flow path for  $\sin \alpha = 1.0$ .

Figure 9. - Continued. Second group of numerical examples, showing effect of diffuser wall spacing as affected by changes in compressor flow coefficient  $\phi$ .



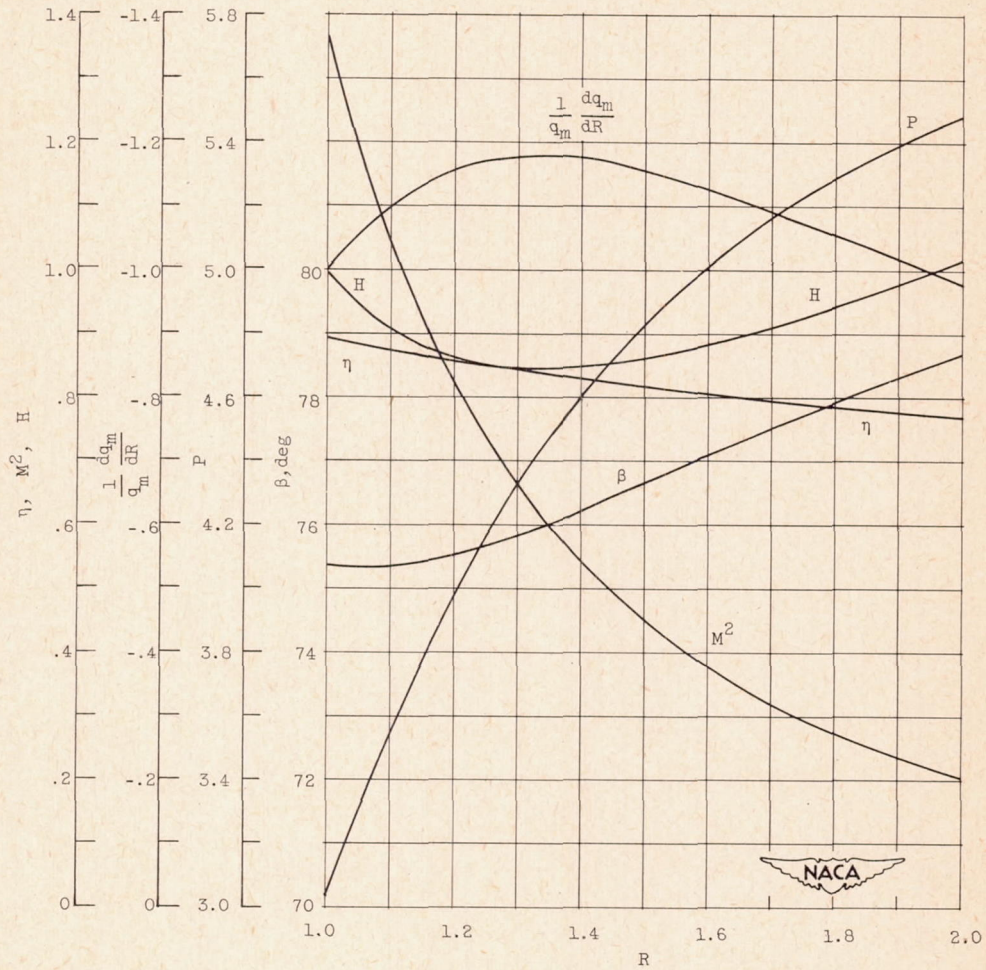
(e) Variation in polytropic efficiency with radius.

Figure 9. - Continued. Second group of numerical examples, showing effect of diffuser wall spacing as affected by changes in compressor flow coefficient  $\phi$ .



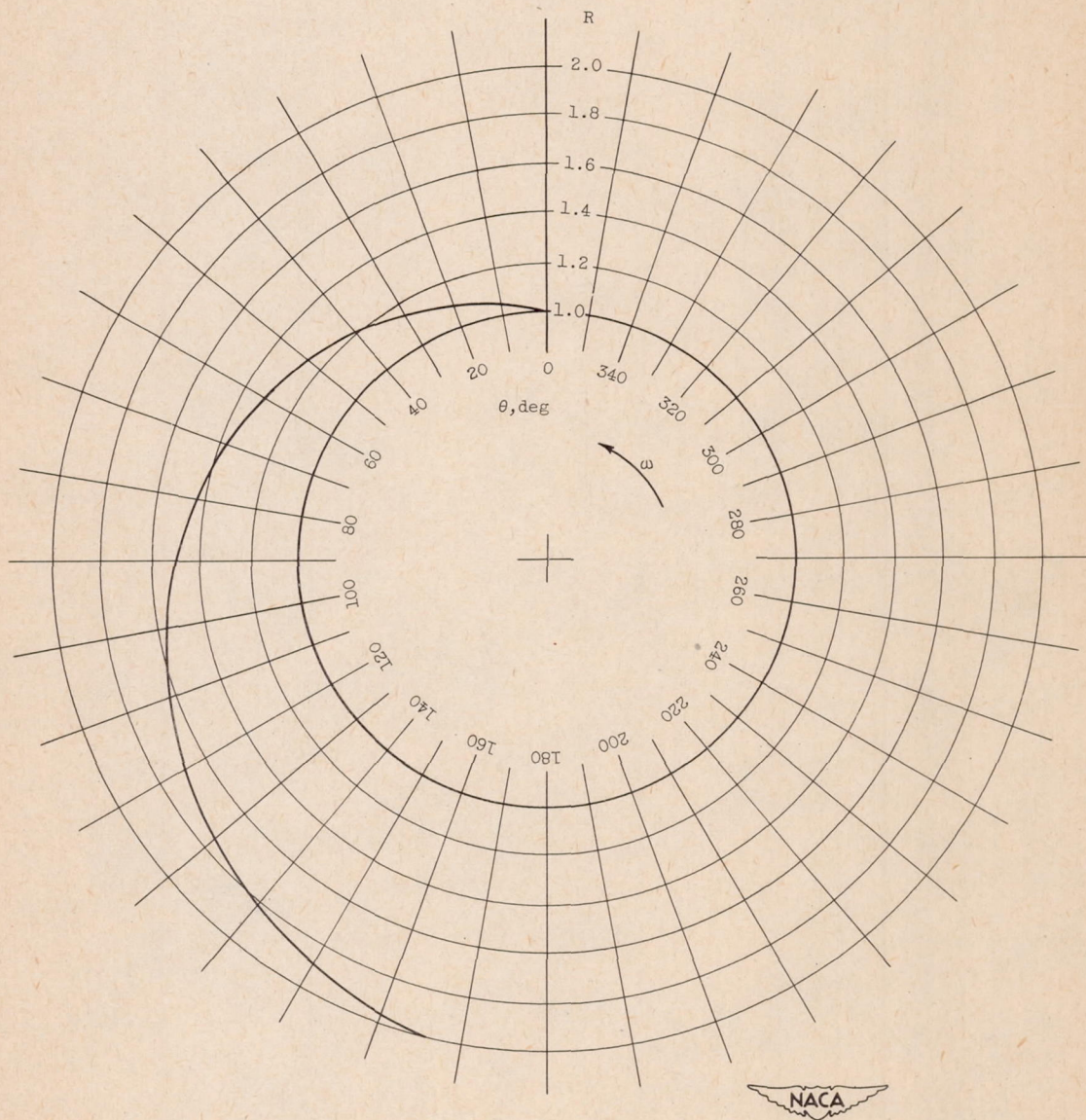
(f) Variation in vaneless diffuser efficiency  $(\eta_D)_2$  with compressor flow coefficient.

Figure 9. - Concluded. Second group of numerical examples, showing effect of diffuser wall spacing as affected by changes in compressor flow coefficient  $\phi$ .



(a) Variation in flow conditions with radius.

Figure 10. - Design problem.



(b) Flow path for  $\sin \alpha = 1.0$ .

Figure 10. - Concluded. Design problem.